J Neurophysiol 89: 2726–2742, 2003;
10.1152/jn.00550.2002.

Space-Time Maps and Two-Bar Interactions of Different Classes of Direction-Selective Cells in Macaque V-1

Bevil R. Conway and Margaret S. Livingstone
Department of Neurobiology, Harvard Medical School, Boston, Massachusetts 02115

Submitted 11 July 2002; accepted in final form 3 December 2002

Conway, Bevil R. and Livingstone, Margaret S. Space-time maps and two-bar interactions of different classes of direction-selective cells in macaque V-1. *J Neurophysiol* 89: 2726–2742, 2003; 10.1152/jn.00550.2002. We used one-dimensional sparse noise stimuli to generate first-order spatiotemporal maps and second-order two-bar interaction maps for 65 simple and 124 complex direction-selective cells in alert macaque V1. Spatial and temporal phase differences between light and dark space-time maps clearly distinguished simple and complex cell populations. Complex cells usually showed similar direction preferences to light and dark bars, but many of the directional simple cells were much more direction selective to one sign of contrast than the reverse. We show that this is predicted by a simple energy model. Some of the direction-selective simple cells showed multiple space-time-slanted subregions, but others (previously described as S1 cells) had space-time maps that looked like just one subregion of an ordinary simple cell. Both simple and complex cells showed directional interactions (nonlinearities) to pairs of flashed bars (a 2-bar apparent-motion stimulus). The space-time slant of the simple cells correlated with the optimum dX/dT (velocity) of the paired-bar interactions. Some complex cells also showed a space-time slant; the direction of the slant usually correlated with the preferred direction of motion, but the degree of slant correlated with the inferred velocity tuning only when measured by a weighted-centroid calculation. Principal components analysis of the simple-cell space-time maps yielded one fast temporally biphasic component and a slower temporally monophasic component. We saw no consistent pattern for the spatial phase of the components, unlike previous reports; however, we show that principal components analysis may not distinguish between spatial offsets and phase offsets.

INTRODUCTION

In 1959 David Hubel reported that some neurons in the cat's visual cortex respond to a visual stimulus only if it is moved in one direction and not the reverse. Direction-selective cells were later found in the retinas of other mammals, like the rabbit, but they have not been found in the retinas of primates. The mechanism for direction selectivity in retinal ganglion cells is as yet unresolved, although most evidence suggests an asymmetry between excitatory and inhibitory inputs (Taylor et al. 2000; Yoshida et al. 2001). The mechanism for cortical direction selectivity is also not well understood. One might suppose that cortical directional cells inherit their directionality from direction-selective retinal ganglion cells, but direction-selective cells are not found in the primate lateral geniculate nucleus (Dreher et al. 1976; Wiesel and Hubel 1966). Therefore it is more likely that cortical direction selectivity is generated de novo.

One popular model for cortical direction selectivity proposes that at the first stage of direction selectivity, the time course of the response of a directional cell changes progressively across the receptive field in such a way that the response is slower on the "preferred" side and faster on the "null" side (Fig. 1*A*). That motion perception is based on such linear spatiotemporal filters was first proposed in theoretical papers (Adelson and Bergen 1985; Watson and Ahumada 1985). Response maps of such cells when plotted in space and time coordinates would show a slant, and the slant would correspond to the unit's preferred velocity. Because of the space-time slant, stimulating the slower part of the receptive field shortly before stimulating the faster part results in greater overlap in the two responses than when two stimuli are presented in the opposite sequence (Fig. 1*B*). A purely linear filter would give directionality only for peak firing rate in response to a moving bar or response modulation to gratings but not for total spikes in response to a moving bar (Fig. 1*B*).

Direction-selective simple cells in both cat and primate visual cortex can show space-time-slanted receptive fields (DeAngelis et al. 1993; De Valois and Cottaris 1998; De Valois et al. 2000; McLean and Palmer 1989; Movshon et al. 1978a); for many simple cells, the presence of direction selectivity, the direction of preferred motion, and the preferred velocity all correlate well with the receptive-field space-time slant. This correlation has been taken as evidence that the spatiotemporal slant underlies directionality. However, direction selectivity is usually stronger than is predicted by linear mechanisms, which can account for only one-fifth to one-half of the observed directionality (Albrecht and Geisler 1991; McLean and Palmer 1989; Reid et al. 1991; Tolhurst and Dean 1991). Moreover some directional simple cells do not show a space-time slant (Baker and Cynader 1988; Baker 2001; Murthy et al. 1998), so different or additional mechanisms are needed to account for their directionality. A static nonlinearity (a squaring or a thresholding) is usually proposed to enhance the directionality generated by linear mechanisms.

Here we have generated high-resolution space-time maps and sequential two-bar interaction maps for a large number of direction-selective cells in alert macaque V1. We explore how these maps fit with various models for direction selectivity.

Address for reprint requests: Please address correspondence concerning this manuscript to: M. Livingstone, Dept. of Neurobiology, Harvard Medical School, 220 Longwood Ave., Boston, MA 02115 (E-mail: mlivingstone@hms.harvard.edu).

The costs of publication of this article were defrayed in part by the payment of page charges. The article must therefore be hereby marked "*advertisement*" in accordance with 18 U.S.C. Section 1734 solely to indicate this fact.

METHODS

We recorded single units in V1 of three alert fixating macaque monkeys. The monkeys were prepared for chronic recording from V1 under general anesthesia using sterile techniques (Livingstone 1998). The monkeys were trained to keep their gaze within 1° of a small spot to receive a juice reward. Spikes were used for mapping only if the monkey's eyes were within the fixation window at the time of stimulus onset; eye movements during a stimulus presentation are unlikely given that the stimulus durations were 13 ms. Eye position was determined with a scleral eye coil monitored with a magnetic-field coil (CNC Engineering, Seattle, WA). To prevent slippage, the eye coils were sewn to the sclera using fine absorbable sutures. The eye-position monitor has a spatial resolution of 0.05° (mean noise in the absence of a monkey). The eye-position monitoring was calibrated at the beginning of each recording session by having the monkeys look in random order at tiny dots in the center of the monitor and at the corners of a 3–10° square (depending on the eccentricity of the cells recorded). The monkeys had to keep their gaze within the fixation window for 2–4 s to receive a juice reward. During periods of stable fixation, average residual eye movements were less than 0.25°. These residual eye movements were compensated for using eye-position correction (Conway 2001; Livingstone 1998; Livingstone and Tsao 1999; Livingstone et al. 1996). As shown by the maps here and in our previous papers, this technique affords mapping of simple-cell subunit organization in parafoveal V1 and gives reproducible substructure in independent maps obtained from the same cell (Conway 2001; Livingstone and Tsao 1999). All procedures were approved by the Harvard Medical Area Standing Committee on Animals.

Neuronal responses were recorded extracellularly using fine electropolished tungsten electrodes coated with vinyl lacquer (Frederick Haer, Bowdoinham, ME) (Hubel 1957). Units were isolated using a dual-window discriminator (BAK Electronics, Germantown, MD) after they were amplified and band-pass filtered (1–10 kHz). Only well-isolated single units were analyzed. Spikes were recorded at 1,000 Hz, eye position at 250 Hz.

Cortical cells were tested for orientation and direction selectivity using fields of moving oriented bars of optimal length and width. Twenty directions evenly distributed around 360° were presented in pseudorandom order, with at least four presentations of each direction, more if the tuning curve was unclear. A direction index (DI) was calculated from responses to optimally oriented single bars moving back and forth at the optimum speed and orientation

$$\mathrm{DI} = (R_p - R_n)/(R_p + R_n)$$

where R_p is the response (total spikes per sweep) in the preferred direction and R_n is the response in the null direction. Cells were tested with both light and dark bars (on a gray background) of optimum length and width. At least five sweeps in each direction were averaged; the sweep excursion was long enough that as long as the animal's eye position was within the gaze box, the termini of the

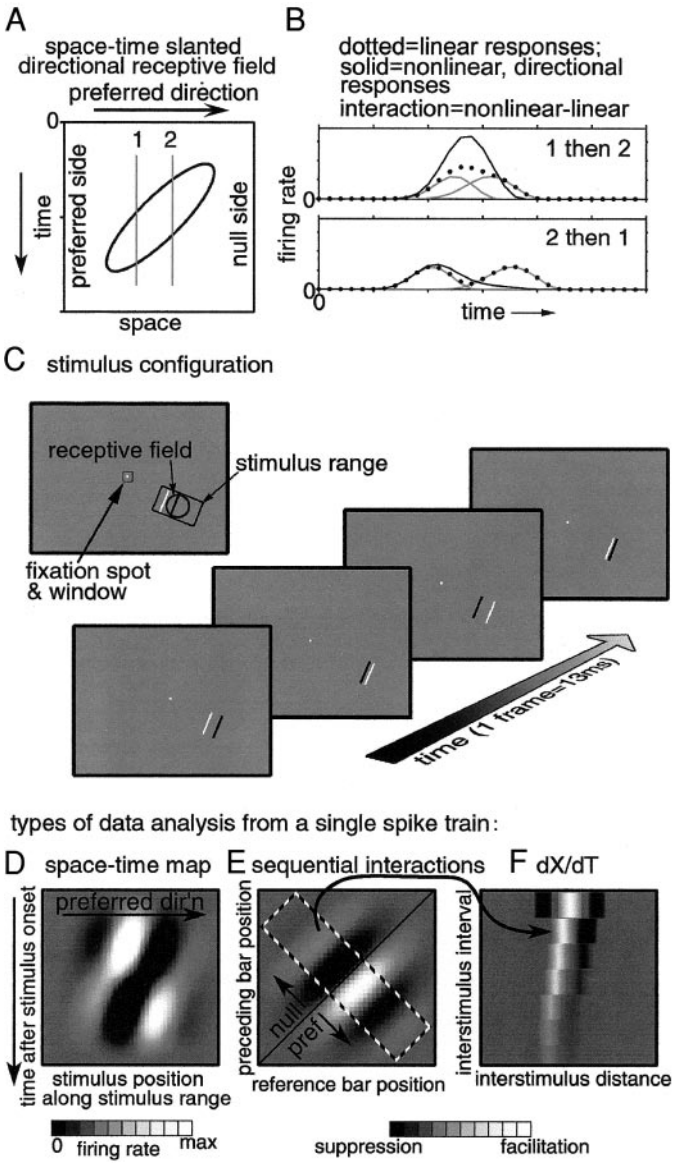

FIG. 1. Background for the experiments described in this paper. *A*: diagrammatic space-time map of a linear direction-selective simple cell with space-time slant, plotted with the preferred direction of movement represented as rightward on the horizontal axis. 1 and 2 are 2 positions in the cell's receptive field. The "preferred" side of the receptive field is the side from which preferred motion originates, according to the conventions of He and Masland (1997). *B*: if the perfectly linear cell in *A* was stimulated by bars presented at positions 1 and 2 in the preferred-direction sequence, the peak firing rate would be higher than if the same two stimuli were presented in the null-direction order, but the total spikes for the two directions would be the same (· · ·). A cell gives a directional response (total spikes in the preferred direction > total spikes in the null direction) if it combines responses nonlinearly (—). The "interaction" between the 2 stimuli is the difference between the · · · and —. *C*: stimulus configuration for the experiments in this paper. While the monkey fixated, pairs of bars, 1 white, 1 black, were presented each frame at 75 Hz along a stimulus range perpendicular to the cell's preferred orientation. *D*: space-time maps. Firing rate is plotted as a function of stimulus position (corrected for eye position) and time after stimulus onset for each bar contrast. The space-time plots are always oriented so that the preferred direction of motion is rightward on the horizontal axis. The color code is a linear scale of firing rate. The dark-bar response is subtracted from the light-bar response to obtain a composite map. *E*: sequential-interaction maps. Spike activity is reverse correlated with pairs of sequentially presented stimuli. For every pair of stimuli, the second is considered the reference, and the first stimulus is considered the probe stimulus. Reference stimulus position (corrected for eye position) is plotted along the horizontal axis (rightward corresponds to the preferred direction) and probe stimulus position is plotted along the vertical axis (upward corresponds to the preferred direction). Points along the +45° diagonal correspond to occasions when the 2 sequential stimuli fell on the same retinal location (no motion); points to the right of the diagonal correspond to preferred-direction sequences and points to the left to null-direction sequences. The color code corresponds to nonlinear interaction strength. *F*: d*X*/d*T* maps. These maps show interaction strength as a function of interstimulus distance (horizontal axis) and interstimulus interval (vertical axis). The interstimulus interval represents the number of frames between the pairs of stimuli with which the activity is reverse correlated. Activity is always mapped at the peak of the reference stimulus response. To obtain these maps, −45° slices covering the interaction region (indicated by dotted rectangle in *E*) are averaged from sequential interaction maps generated using different interstimulus intervals. As with the interaction maps, the color scale indicates nonlinear interaction strength.

sweep were outside the cell's activating region; sweeps were averaged only if the animal's gaze remained inside the gaze box for the entire duration of the bidirectional sweep. Cells that gave a 50% greater response to movement of the bar in one direction over movement of the bar in the opposite direction (DI $>$ 0.2), for either contrast bar, and did not show opposite direction preference for light and dark bars were accepted as direction selective.

Stimulus sequences from which we determined space-time maps and paired-stimulus interactions

While the monkey fixated, pairs of optimally oriented bars, one black and one white, were flashed simultaneously on a gray background, at random positions along a stimulus range that was perpendicular to the bar orientation (Fig. 1*C*). This stimulus was designed to allow us to obtain both the space-time maps (1st-order analyses) and paired-bar interaction maps (2nd-order analyses) from a single stimulus run. This is the sparsest stimulus that allows us to do this. The monitor was 75 or 100 cm from the monkey, depending on the set up, and had a 75-Hz refresh rate. Stimulus presentation rate was 75 Hz. Stimuli were presented monocularly to the dominant eye [using colored stimuli and filters (Livingstone and Tsao 1999)] or binocularly (without colored filters) if there was no difference in the receptive fields in the two eyes. White and black stimuli were 19cd/m^2 above and below the mean background luminance of 20 cd/m^2. The overlap of the black-and-white stimuli appeared as the background gray. For each map, between 5,000 and 50,000 spikes were collected over a 5- to 30-min period. Using this stimulus configuration, we calculate, from a single spike train, space-time maps to each contrast, sequential interaction maps, and dX/dT maps (Fig. 1, *D–F*). Space-time maps (Fig. 1*D*) were smoothed with a two-dimensional Gaussian low-pass filter with a sigma of 3 ms in the temporal dimension and 0.1° in the spatial dimension. Sequential interaction maps (Fig. 1*E;* which are space-space maps) were smoothed with a 0.1° wide Gaussian in both spatial dimensions.

Space-time maps

From a continuous record of stimulus position, eye position, and neural activity, we calculated the average response to one contrast bar, at every spatial position along the stimulus range, independent of the location of the opposite-contrast bar. All the space-time maps are oriented so that rightward on the space (horizontal) axis corresponds to the preferred direction of stimulus motion (Fig. 1*D*). Each stimulus position was corrected for the monkey's eye position at stimulus onset (Livingstone 1998).

There is often a dark band apparent to either side of the excitatory response in the space-time maps; these dark bands do not necessarily represent inhibitory side bands. The dark bands reflect the firing rate at the peak latency produced by frames when the stimulus was outside the activating region, whereas the higher firing at earlier and later times corresponds to the firing rate averaged over the entire stimulus range, including the activating region. In other words, in the space-time maps, activity is mapped as a function of stimulus position at time = 0, but there are many stimulus presentations before and after that stimulus, and some of them land in the cell's receptive field. So, if one calls the stimulus latency L and optimal position P, because the maps are keyed to the stimulus presented at *time 0*, the response at time L and positions other than P will be baseline. But at all other times and positions, there is a finite probability that the stimulus occurring L ms previously was the optimal one, and so there is a finite, noisy background at these times. Difference space-time maps were generated by subtracting the dark-bar map from the light-bar map (Movshon et al. 1978a).

To categorize cells as simple or complex, we quantified the space-time receptive-field organization. We determined the temporal and spatial receptive-field profiles for the responses to dark and light bars. The temporal profile was averaged over 0.12° of visual angle; the spatial profile was averaged over 10 ms, both centered on the peak of the response (the peak of the dark or the light-bar response, whichever was bigger). The spatial and temporal profiles for each contrast were fit to a Gabor function (a Gaussian times a cosine wave)

$$f(x) = A \exp(-(x - c)^2/(2\sigma^2)) \cos(2\pi\upsilon(x - c) + \phi) + \Omega$$

where A is the amplitude, c is the center, σ is the SD of the Gaussian, υ is spatial frequency of the sinewave, ϕ is the phase of the cosine wave, and Ω is the baseline offset.

The fits were constrained so that the Gabors for both light and dark maps had the same center and spatial frequency. The center and spatial frequency actually used were the average of the optima for each profile fit independently. (Unless, as in the 1-subunit simple cells, see following text, a profile for one contrast was so flat that it was essentially noise, in which case the stronger profile was used to determine the center and spatial frequency.) The σ of the Gaussian was at least one full cycle of the sinewave (so the width of the Gaussian was at least 2 full cycles). Although the Gabor used was much wider than the best-fitting Gabor would be, it allowed us to determine the relative positions of the light and dark subregions with a single parameter, the phase of the cosine. We fit the profiles to a wide Gabor rather than to just a sinewave so that the fit would be driven predominantly by the activating region rather than by the regions outside the receptive field. The fits were optimized via a least-squares criterion with the Levenberg-Marquardt algorithm in Matlab (Mathworks, Natick, MA). The phases of the sinusoids of the best-fitting Gabors were compared for the light and dark stimuli. Phase is defined as the phase of a cosine wave having the same center as the Gaussian. We recorded from five cells that responded to only one sign of contrast; these cells were not included in the population because we could not distinguish them as simple or complex.

Some cells had space-time maps that looked like one subregion of a mulitple subunit simple cell. We treat these cells separately in our analyses, even though we observed a range of subunit number, because they do not fit the original definition of simple cells (Hubel and Wiesel 1962). Cells were categorized as one-subunit simple cells if they showed complementarity between light and dark-bar responses but throughout the response had only one spatial subregion. Whether a cell had more than one subregion was determined by comparing the magnitudes (positive or negative) of the peaks in the spatial profile; a peak counted as another subunit if it was at least 10% the magnitude of the major peak. These one-subunit simple cells correspond to the S1 cells described by Schiller et al. (1976), who categorized cells using moving light and dark edges.

Principal components analysis was done on the space-time maps of simple cells using the Matlab code for singular value decomposition. For the first two principal components of each simple cell, the magnitude of the largest peak (positive or negative) and the magnitude of the following peak were measured. The timing of the major peaks was compared for the first two principal components, and the component whose major peak reached maximum first was considered the "fast" component, and the other was the "slow" component. The biphasic index for each principal component is the ratio of the second temporal peak divided by the first (De Valois et al. 2000). A biphasic index near 1 indicates a biphasic temporal profile and indices near 0 correspond to monophasic profiles. To measure the spatial organization of the first two components for each cell, the spatial profile through the largest peak was fit with a Gabor. The phase of the cosine wave was taken as the spatial phase; even symmetric profiles had phases near 0° and odd symmetric profiles had phases near 90°.

Two-bar interaction maps (Wiener-like kernels)

From the same spike train used to generate the first-order space-time maps, we could also map activity as a function of paired-stimulus

sequences (Fig. 1*E*). This is a novel way of looking at directional interactions at a single interstimulus interval. In describing the sequences, the second stimulus of each pair is called the reference stimulus. Each stimulus position was corrected for the monkey's eye position at stimulus onset (Livingstone et al. 1996). We plotted interactions as a function of reference stimulus position (horizontal axis) and preceding stimulus position (vertical axis). Thus nonlinear interactions are mapped in space/space coordinates, but the coordinates are not two-dimensional (2-D) visual space but rather paired-bar position coordinates. Interactions were plotted at a temporal delay corresponding to the time to peak response for the reference stimulus (between 45 and 60 ms). In the sequential interaction maps, the +45° diagonal indicates occasions when the two sequential stimuli appeared at the same location (no motion). The maps are oriented so that rightward on the horizontal axis and upward on the vertical axis correspond to the preferred direction of stimulus motion. Therefore regions below/right of the green diagonal represent two-bar sequences in which the stimuli were presented in the preferred direction, and regions above/left of the diagonal represent null-direction sequences. Increasing distance from the +45° diagonal corresponds to increasing interstimulus distance.

From one spike train, we mapped responses to all four combinations of two-bar sequences: white-to-white, black-to-black, white-to-black, and black-to-white. To look at *interactions* between pairs of stimuli, we want to know what aspects of a paired-bar response depend on the pairing of the stimuli and which depend on the responses to the two stimuli presented independently. Interactions are those parts of the paired-bar response that depend on pairing, so have the linear or independent responses to the two stimuli subtracted from the paired-stimulus response (Fig. 1*B*). One way to do this is to subtract the inverting-sequence maps (white-to-black and black-to-white) from the summed same-contrast sequences (white-to-white and black-to-black) (Emerson et al. 1987); these difference maps show only those aspects of the sequential response that depend on stimulus order or position. Subtracting the inverting-contrast responses from the same-contrast responses eliminates the first-order (linear) responses, leaving only the nonlinear interactions. This is equivalent to calculating a second-order Wiener-like kernel (Emerson et al. 1987) in two-bar position coordinates. Any deviation from 0 in the interaction maps must be attributable to the fact that the stimuli were presented sequentially and not independently; these maps are equivalent to the difference between the observed response to two-bar apparent motion and the linear sum of the responses to the two stimuli presented independently. The mapping technique is a generalization of the two-bar interaction maps of Movshon et al. (1978b), and the maps are analogous to the binocular interaction maps of Ohzawa et al. (1997) except interactions are mapped as a function of the position of two sequentially presented bars rather than as a function of stimulus position in each eye. In our maps, positive interactions (same-contrast facilitation and inverting-contrast suppression) are indicated in red and negative interactions (same-contrast suppression and inverting-contrast facilitation) in blue.

dX/dT maps

To show the evolution of the nonlinear directional interactions at a series of interstimulus intervals in a single d*X*/d*T* map (Fig. 1*F*), we first calculated (for each interstimulus interval) a two-bar interaction profile from two-bar interaction maps just as described in the preceding text. For simultaneously-presented stimuli, we have only inverting-contrast sequences and no same-contrast sequences, so the nonlinear simultaneous interactions were calculated by subtracting maps generated using long (250 ms) interstimulus intervals from the 0-ms maps (Livingstone et al. 2001). For each interstimulus interval, we generated one-dimensional profiles of interaction strength as a function of interstimulus distance by averaging the interactions for every interstimulus distance (Livingstone et al. 2001) across a slice running parallel to the −45° diagonal, encompassing the interaction region. This gives the average paired-stimulus interactions as a function of interstimulus distance, and the slices are then stacked to give interactions as a function of interstimulus distance and interstimulus interval. This analysis is similar to that used by Emerson et al. (1987); they refer to their d*X*/d*T* maps as "motion kernels."

Measuring the slant of space-time maps

We compared three ways of calculating the space-time slope and settled on using a weighted centroid calculation, similar to the calculated used by McLean and Palmer (1989), but with each point weighted by the response magnitude. In RESULTS, we discuss why this is an appropriate calculation for the paired-bar stimulus we used. We calculated the weighted mean position (centriod) in space for each ms for ±15 ms on either side of the peak response using the following equation (McLean and Palmer 1989)

$$\text{centroid at time } t = \left\{\sum x^{*}z(x, t)\right\} \Big/ \left\{\sum z(x, t)\right\}$$

where x = spatial position and z = firing rate at position x at time t.

We calculated the best fitting line for the centroids in a different way, however, from McLean and Palmer (1989) in that we used a maximum likelihood estimation to fit a line, and used the width (sigma) of the best-fitting Gaussian for each millisecond-long time slice ±15 ms from the peak as an estimate of the SD of the peak value. We wanted to weight each centroid by the magnitude of its response. Maximum likelihood estimation fits a line weighting each data point by its SD, with points with small SDs being weighted more. For our time slices, the width of a best-fitting Gaussian will be inversely related to the peak height.

The second way we calculated the slant of the space-time maps was to find the angle giving the maximum peak in a Radon transform (Deans 1983) of the white or dark bar response map, whichever was larger. To do this, we first subtracted the baseline activity and set to zero any below-baseline regions. The Radon transform gives the image intensity summed along image slices taken at different angles. Thus the peak of the Radon transform gives the angle of a line that maximizes image intensity. The third way we calculated the slant of space-time maps was from the peak of the Fourier transform of the space-time map.

Modeling

To generate the models in Figs. 8, 10, and 11, two nondirectional cells (a fast one and a slow one) were calculated by multiplying a spatial Gabor function and a temporal function. The spatial Gabor for the slow nondirectional cell was 90° phase-shifted from the fast component in Figs. 8 and 11, and in Fig. 10, the center position was shifted, but not the phase. We used temporal functions similar to those used by Adelson and Bergen (1985)

$$f(t) = (kt)^{n} \exp(-kt)[1/n! - (kt)^{2}/(n + 2)!]$$

where $n = 17$ for the fast component and $n = 21$ for the slower component. For the monophasic model, the slower component was rectified so that it had only the first, positive-going phase. Responses to pairs of stimuli were rectified then squared. Direction indices were calculated by summing every possible paired-bar response, assuming a 5-ms interval between stimuli. Nonlinear interactions were calculated in two ways: by subtracting inverting-contrast responses from same-contrast responses (2nd-order Wiener kernels) or by summing sequential responses then rectifying and squaring (Heeger 1992), then

subtracting the independently rectified then squared sum of the same responses.

RESULTS

We recorded the activity of single units in primary visual cortex (V1) of three macaque monkeys. For each cell, we first determined the preferred stimulus orientation and direction using moving bars. A direction index, DI, was calculated for both light and dark bars. Cells were considered directional if they had a DI > 0.2 for one stimulus contrast and did not show the opposite direction preference for the opposite stimulus contrast. In an earlier study from this laboratory (Livingstone 1998), a more stringent criterion was used to accept cells as directional (DI >0.5 for *both* stimulus contrasts), and almost no simple cells meeting that criterion were found. As discussed in the following text, this difference in directionality for black-and-white bar stimuli is to be expected from the energy model. By relaxing our definition of direction selectivity, we were able to identify directional simple cells with slanted space-time maps similar to those previously described in the cat (DeAngelis et al. 1993; McLean and Palmer 1989; Murthy and Humphrey 1999) and monkey (De Valois and Cottaris 1998; De Valois et al. 2000). After identifying a unit as direction selective, we then mapped the receptive field using the sparse noise stimulus illustrated in Fig. 1*C*.

Space-time maps; simple versus complex cells

From a single spike train recorded during the presentation of 20,000–130,000 stimulus frames (5–30 min), we averaged the response at each retinal position to white bars, disregarding the black bars, or to black bars, disregarding the white bars. Figure 2 shows responses to moving bars and space-time maps for a typical directional complex cell and a typical directional simple cell. The maps for these two cells show several features that seemed to consistently distinguish simple and complex directional cells in our population. We will first describe these differences for this pair of cells, then quantify the differences for the population. First, the complex cell showed strong direction selectivity to both light and dark moving bars (Fig. 2, *A* and *B*). The simple cell, in contrast, was directional to light bars (*G*) but not to dark bars (*H*). Second, the space-time maps of the simple cell showed rough complementarity of light and dark responsive regions (*I* and *J*), but the complex cell did not (*C* and *D*) (Hubel and Wiesel 1962). Third, the simple-cell space-time maps showed an overall slant also as previously described (DeAngelis et al. 1993; De Valois and Cottaris 1998; McLean and Palmer 1989; Murthy and Humphrey 1999). For the complex cell, the space-time maps were not clearly slanted, although there was an asymmetry along the spatial axis with the response being more transient on the right (null) side of the receptive field, with a delayed suppressive response (the darker blue blobs below and slightly to the right of the red blobs) to both light and dark stimuli that was slightly spatially offset, toward the null side of the receptive field, as previously described (Livingstone 1998). Thus in complex directional cells, ON and OFF regions were coextensive, but excitatory and suppressive regions were not necessarily. Fourth, the firing rate was higher for the complex cell than for the simple cell. Last, the complex cell's response was more transient than the simple cell's response.

Simple and complex cells were originally distinguished by Hubel and Wiesel only in the spatial domain (Hubel and Wiesel 1962): complex cells have coextensive light and dark excitatory regions; simple cells have complementary light- and dark-response organization. But simple cells can also be described in the spatiotemporal domain, as having complementary light and dark organization at any point in time (Adelson and Bergen 1985; McLean and Palmer 1989; Movshon et al. 1978a; Watson and Ahumada 1985). To quantify this, we generated spatial and temporal receptive-field profiles (slices in time or space) by determining the activity along the spatial and temporal dimension at the peak response (see METHODS). As shown in Fig. 2, *E* and *F*, for the complex cell, the spatial and temporal profiles for white and black stimuli were similar, but, for the simple cell, the light and dark profiles were complementary (*K* and *L*). For each cell, we fit the light and dark spatial and temporal profiles with a *wide* Gabor function (Fig. 2, *E*, *F*, *K*, and *L*, · · · see METHODS) and measured the phase difference between the sinusoidal components for the light and dark profiles. For the two cells in Fig. 2, the phase difference between the white-bar and black-bar spatial profiles was 11° for the complex cell and 178° for the simple cell; the phase difference between the white-bar and black-bar temporal profiles was 8° for the complex cell and 146° for the simple cell.

We fit Gabor functions to the light and dark temporal and spatial profiles for the entire population of 189 cells. We had qualitatively categorized 124 of these cells as complex and 65 as simple based on the spatial complementarity of ON and OFF responses. The cells that we qualitatively classified as simple had large spatial and temporal phase differences, whereas the cells we categorized as complex had small phase differences (Fig. 3*A*). Some of the cells categorized as simple did not show clear spatial complementarity between light and dark responses (Fig. 3*B*, *middle*) because the response at any point in time was predominantly to only one stimulus contrast and therefore had a well-modulated spatial profile to only one stimulus contrast (1-subunit simple cells, or S1 cells, discussed in the following text). Nevertheless, the temporal phase differences in these one-subunit cells clearly distinguish them as simple, according to the criterion of complementarity between light and dark response regions (Fig. 3*B*).

The complex cell in Fig. 2 was directional to both light and dark moving bars, but the simple cell was not. This was generally true in our population (Fig. 3, *C* and *D*). Figure 3*C* is a scatter plot of the DIs for each cell for black and white moving bars. The fact that the simple-cell data points tend to cluster along the axes (where 1 or the other DI is 0), indicates that many of the simple cells were directional to only one stimulus contrast, while most of the complex cells were directional to both contrasts. Figure 3*D* shows histograms of the ratio of the DI for the poorer contrast to the DI for the better contrast. Relatively more of the simple cells had a DI for one contrast that was much lower than the DI for the other contrast, and relatively more complex cells had balanced DIs for the two contrasts. A similar distinction has been reported in the cat (Goodwin and Henry 1975; Henry 1977). The fact that many directional simple cells in primate V1 are strongly directional to only one stimulus contrast explains why we (Livingstone 1998), and perhaps others (Hubel and Wiesel 1968), missed them in previous studies. Later, we show that a simple model predicts this result.

The simple cells also had, on average, lower baseline firing rates than the complex cells [11 $\pm$ 7 (SD) spikes/s vs. 40 $\pm$ 56.0 spikes/s]. This rate is not the completely unstimulated firing rate but reflects the average response to the stimuli over the entire stimulus range, most of which was outside the cells' activating region. This confirms an observation of Schiller et al. (1976). Because our study was done in alert animals, we can conclude that this difference in baseline firing cannot be attributed to differential sensitivities of simple and complex cells to anesthetic.

Direction-selective simple cells

We observed a range of simple and complex cells that correspond with cells previously described in cat and monkey. Because it has been suggested that complex cells are generated by combining inputs from several simple cells (Hubel and Wiesel 1962) and because receptive-field size varies with ec-

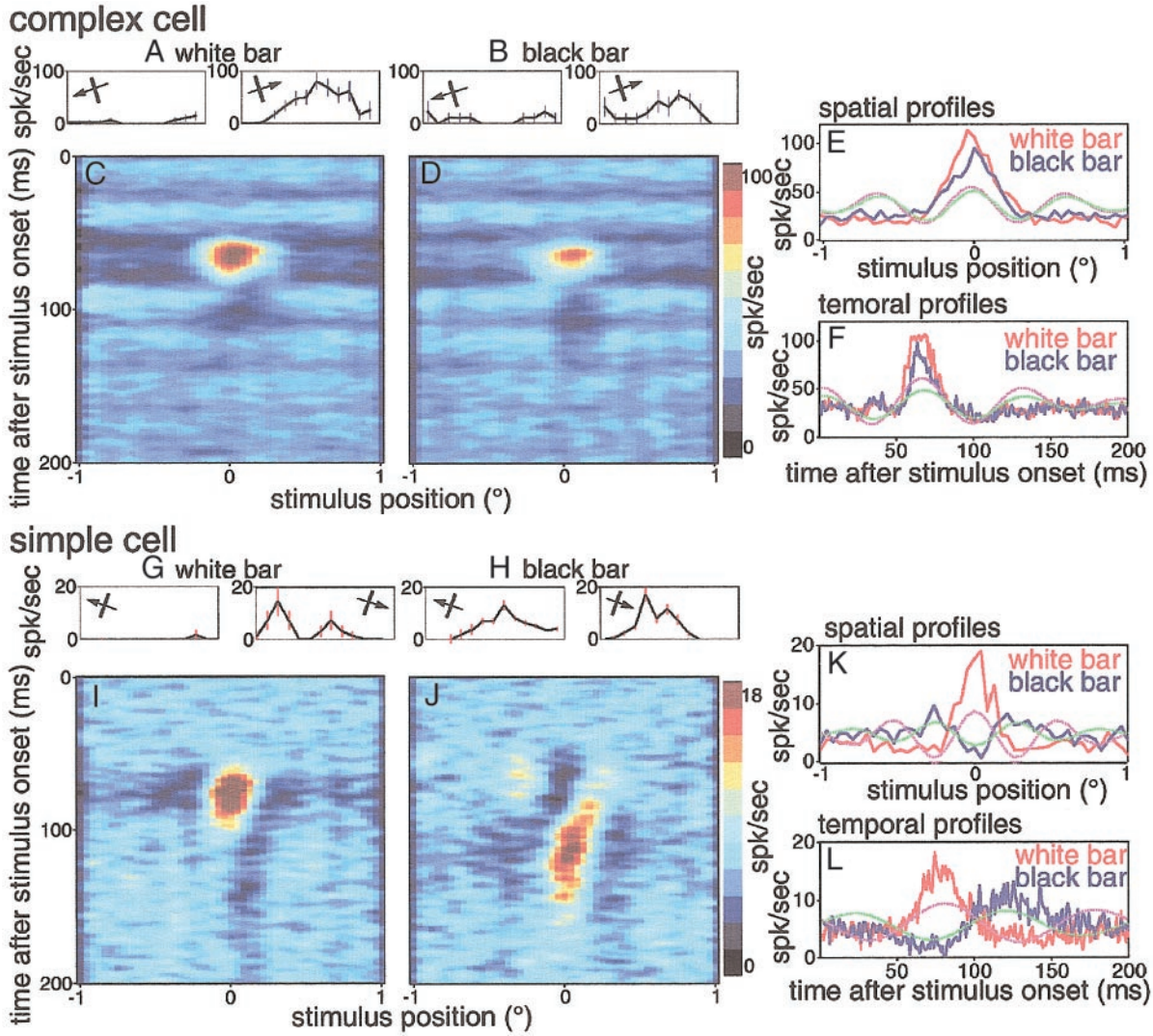

FIG. 2. Representative complex cell and simple cell. *A*, *B*, *G*, and *H*: graph showss each cell's response to a moving white or black bar. The complex cell was strongly directional to both white and black bars, but the simple cell was directional only to white bars. *C*, *D*, *I*, and *J*: space-time maps for white and black bar stimuli. For both cells, the preferred direction of stimulus motion is represented as rightward on the horizontal axis. The horizontal striations in the maps reflect the time course of the stimulus-driven elevation in activity in response to stimulus presentations other than the 1 whose onset was at time = 0. *E*, *F*, *K*, and *L*: spatial and temporal profiles calculated by averaging over ±10 ms and ±0.12°, respectively, centered on the peak response to white bars (because for both these cells the larger response was to white bars). Green and purple lines indicate the best-fitting phase of a wide Gabor for each profile. The 95% confidence intervals for the best-fitting phase for the simple-cell white spatial profile were ±15°; for the dark spatial profile, ±25°; for the white temporal profile, ±11°; for the dark temporal profile, ±12°. The 95% confidence intervals for best-fitting phase for the complex-cell white spatial profile were ±12°; for the dark spatial profile, ±22°; for the white temporal profile, ±23°; for the dark temporal profile, ±12°.

centricity, we thought it might be informative to compare simple and complex cell receptive fields from a small range of eccentricities. The following figures show examples of each of these kinds of cells, all from the same eccentricity. Of the total population, 40 simple cells and 59 complex cells having eccentricities between 1.5 and 3° were recorded from one 2-mm craniotomy in one monkey. The cells in Figs. 4–7 were from this subset of the entire population.

Figure 4 shows five "conventional" directional simple cells with multiple, spatiotemporally slanted subregions. Forty of the 65 simple cells were like this, showing two or more adjacent ON and OFF subregions over most of the response duration. Light-bar excitation and dark-bar suppression occurred in one set of subregions with dark-bar excitation and light-bar suppression in the other, spatially and temporally complementary, subregions (Ferster 1988; Hubel and Wiesel 1962). The light-minus-dark maps (*3rd column*) make clear the overall slant in the space-time maps as previously described in cat and monkey (DeAngelis et al. 1993; De Valois and Cottaris 1998; De Valois et al. 2000; McLean and Palmer 1989; Murthy and Humphrey 1999).

The *first three columns* in Fig. 4 show first-order space-time maps; the *fourth* and *fifth columns* show second-order interaction maps, maps that show the nonlinear interactions between pairs of stimuli. The *fourth column* in Fig. 4 shows the directional interaction maps at 13-ms interstimulus intervals for each cell. As discussed in the preceding text, directionality to two-bar sequences must be entirely nonlinear even if it is based

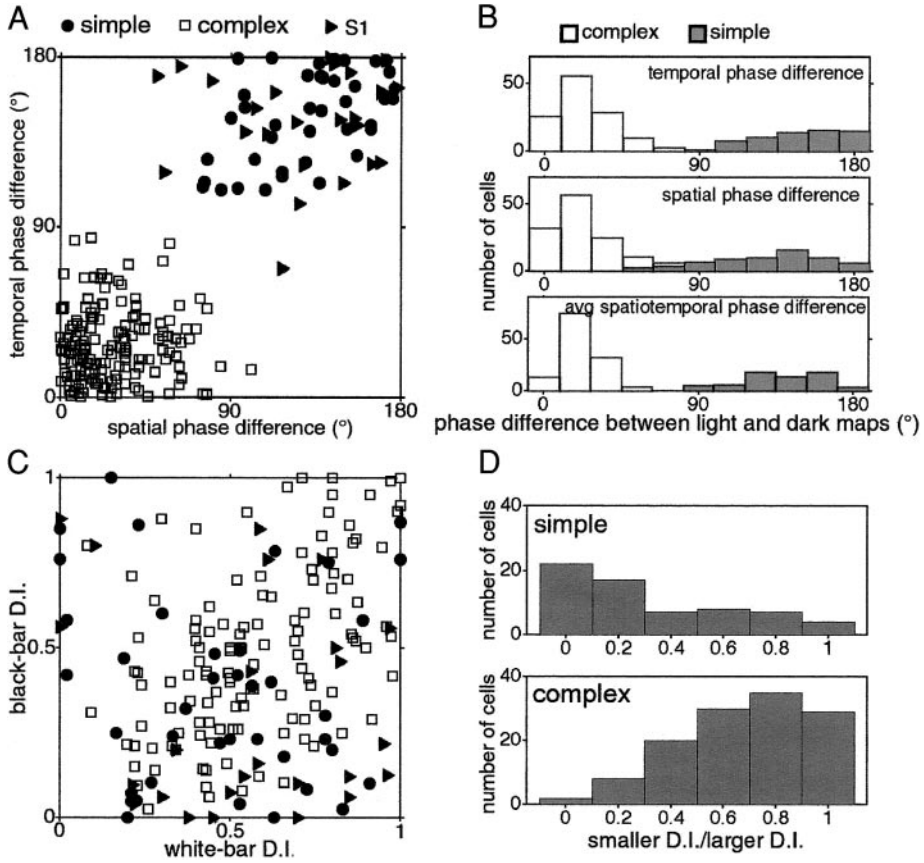

FIG. 3. Various parameters measured for simple and complex directional cells. *A*: spatial and temporal phase differences for light and dark stimuli space-time maps for simple and complex cells (symbols indicate classification by qualitative assesment). *B*: histograms of temporal, spatial, and averaged spatial and temporal phase differences for the population of cells, showing that light/dark spatial and temporal phase differences distinguish simple from complex cells. *C*: direction indices to light and dark moving bars. *D*: ratio of light-bar or dark-bar direction index (DI; whichever is smaller) to DI for the other contrast.

on nonlinear amplification of underlying linear processes. Therefore the directionality must be reflected in the nonlinear interactions between pairs of stimuli. As described in METHODS, in the interaction maps, activity is reverse correlated with the position of each reference stimulus (mapped along the horizontal axis) and with the position of an immediately preceding (13 ms) bar position (mapped along the vertical axis). Positions in this two-bar space along the +45° diagonal represent occasions when the two sequentially presented bars fell on the same retinal location (no motion); positions to the right of the diagonal represent preferred-direction sequences, and positions to the left represent null-direction sequences. All of the cells in Fig. 4 showed a preponderance of facilitatory interactions in the preferred-direction region of the map and suppressive interactions in the null-direction region. Many of the maps show a checkerboard arrangement of facilitatory and suppressive interactions, which, as discussed in the following text, is predicted by several models for direction selectivity. In the binocular interaction maps of Ohzawa et al. (1997), which are similar in principal to our sequential interaction maps, simple cells similarly show checkerboard interaction patterns. The checks represent interactions between and within individual subunits of the simple cells.

The sequential interaction maps in the *fourth column* of Fig. 4 show interactions at one interstimulus interval—13 ms (at every possible position of each stimulus)—because they are generated by correlating activity with pairs of bars in sequential frames. But we can also generate similar maps correlating activity with pairs of bars separated by two, three, or more frames. To look at interaction strength as a function of both interstimulus interval and interstimulus distance, we averaged a slice of each interaction map running parallel to the −45° diagonal for a series of interstimulus intervals (*5th column*, Fig. 4). In these graphs, negative interstimulus distances correspond to the preferred direction. At 0 ms (simultaneously presented stimuli), there is, by definition, no directionality, and the interactions are symmetrical about 0. The interaction pattern shifts abruptly from symmetry (at 0 ms) to showing facilitation for preferred-direction sequences and suppression for null-direction sequences in the 13-ms interstimulus interval slice. The dX/dT maps show an overall slant, although it is not necessarily a straight line: in the slice corresponding to an interstimulus interval of two frames (27 ms), the facilitatory peak is at a larger interstimulus distance than it is at 13 ms, although for most of the cells this distance is less than twice the optimum interstimulus distance for 13-ms interstimulus intervals. This slant should correspond to the cells' velocity preferences, but we did not actually test this using moving bars. If direction selectivity (a 2nd-order property) derives from the slant of simple cell spatiotemporal response functions (a 1st-order property), the two should be correlated (Adelson and Bergen 1985). Below we compare the slant of the (1st-order) space-time maps with the initial slant of the (2nd-order) dX/dT maps.

Figure 5 shows cells that had spatially antagonistic light and dark responses yet would not fit the original definition of simple cells of having separate ON and OFF subdivisions (Hubel and Wiesel 1962). However, Schiller et al. (1976) extended the definition of simple cells to include cells with only one contrast-opponent region, which they called S1 cells (Henry 1977;

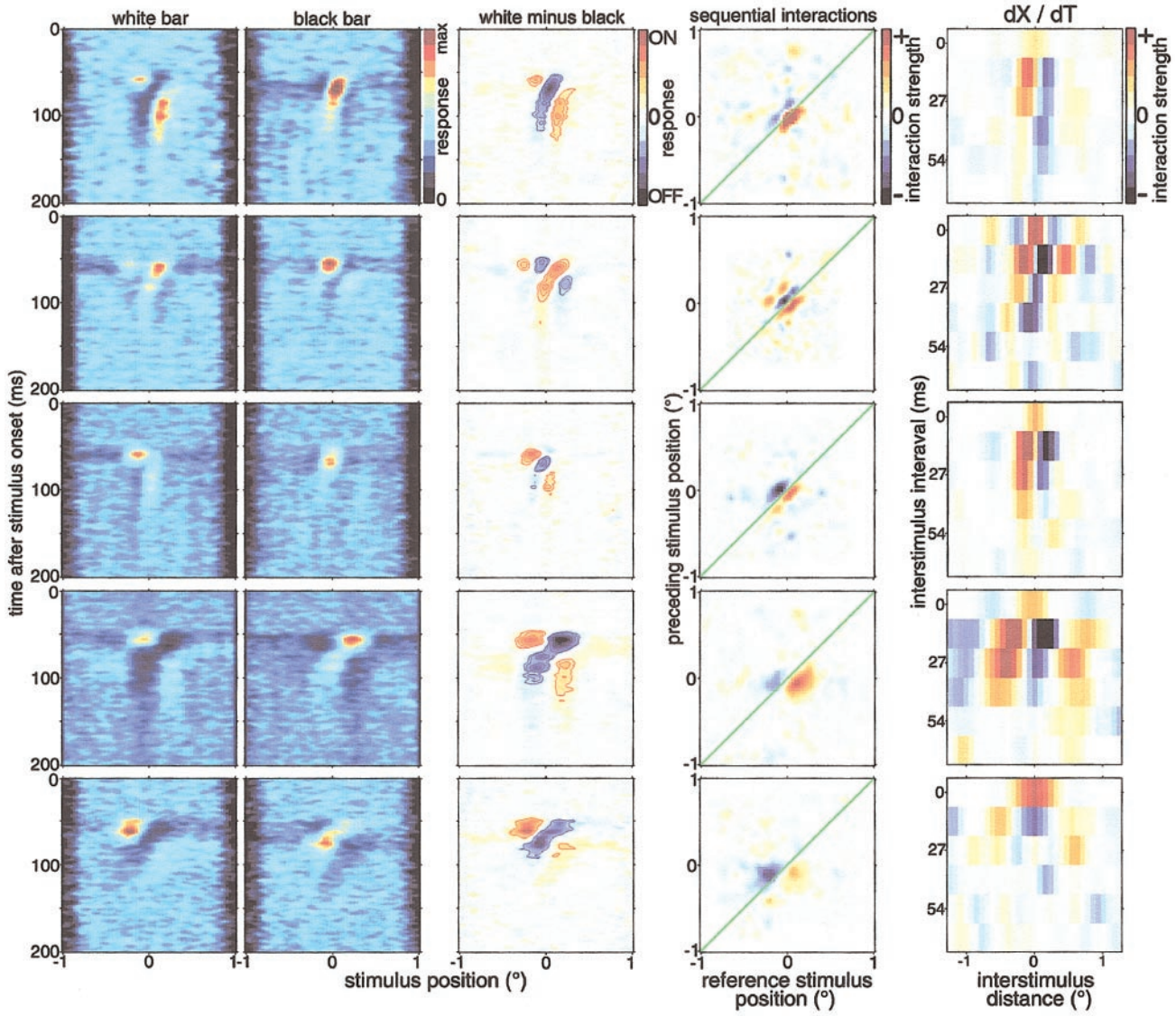

FIG. 4. Space-time maps, sequential interaction maps, and d*X*/d*T* maps for 5 conventional direction-selective simple cells. Each row represents one cell. All these cells had receptive-field eccentricities between 1.5 and 3°. For each spatial axis, the positive direction corresponds to the preferred direction of stimulus motion. *First column*: the space-time map to light bars; *second column*: the space-time map for dark bars; *third column*: the light-bar map minus the dark-bar map; *fourth column*: the 2-bar sequential interaction map for pairs of stimuli presented in sequential frames (13-ms intervals). Below/right of the green diagonal represents preferred-direction sequences and above/right represents null-direction sequences. *Fifth column*: the average interaction strength (calculated from a series of interaction maps) as a function of interstimulus interval.

Schiller et al. 1976). Twenty-five directional cells that fell into the simple-cell category based on spatial and temporal phase differences (Fig. 3*A*) did not have multiple subregions. These cells showed complementarity between light and dark responses but had only one spatial region at most latencies. This single region is organized in a push/pull fashion and looks like a single subregion of a conventional simple cell. We, and others (Schiller et al. 1976), regard them as the simplest form of directional simple cell because it is easy to imagine constructing a conventional, multisubunit, simple cell from several S1 cells.

Like the other simple cells in this study, the single-subunit simple cells were direction selective, but, like the S1 cells described previously (Schiller et al. 1976), they were usually responsive only to one stimulus contrast. The cells in Fig. 5 were directional to moving white bars but unresponsive or nondirectional to moving black bars. (To flashed black bars, these cells showed suppression followed by an OFF discharge; thus they were less responsive to moving dark bars than to flashed dark bars.) The contrast to which a given S1 simple cell was most directional was always the same as the contrast that gave the early excitatory response.

The space-time maps of the S1 simple cells were usually not as clearly slanted as the simple cells with more subunits, yet these cells were direction selective. The nonlinear directional interactions of the S1 simple cells were dominated by null-direction suppressive interactions unlike the conventional simple cells, which generally showed both preferred-direction facilitation and null-direction suppression. The second-order d*X*/d*T* maps of the S1 cells were slanted, even though the

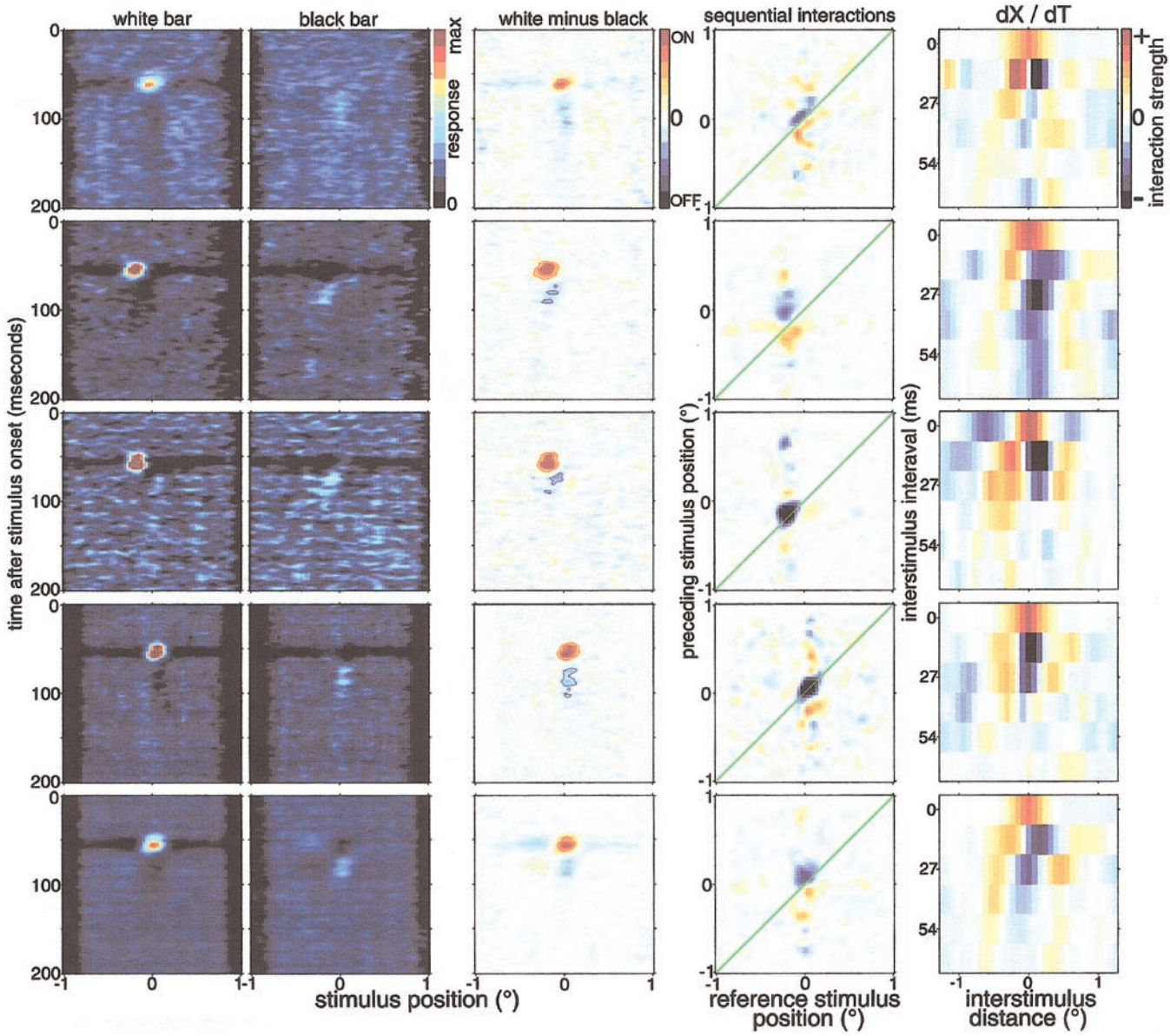

FIG. 5. Space-time maps, sequential interaction maps, and d*X*/d*T* maps for 5 direction-selective 1-subunit (S1) simple cells. All these cells had receptive-field eccentricities between 1.5 and 3°. Conventions as in Fig. 4.

space-time maps were not clearly slanted. Some directional cells in the cat also have been reported to show slanted interaction maps without having slanted space-time receptive fields (Baker 2001).

We have also mapped directional cells that turned out to be intermediate between one-subunit simple (S1) cells and conventional simple cells in that they have one dominant spatial subunit and a second much weaker subunit. That simple cells show a continuous distribution of subunit number is supported by a unimodal distribution of subunit number (data not shown).

We saw many simple cells that showed opposite direction preferences for light and dark bars. Their space-time maps consisted of a temporally biphasic ON region adjacent to a temporally biphasic OFF region. These simple cells, similar to those originally described by (Hubel and Wiesel 1962), preferred movement of a white bar from the OFF region into the ON and movement of a black bar from the ON region into the OFF region. We did not include these cells in our population of directional cells because they showed opposite directionality for light and dark stimuli. Nevertheless it is worth pointing out that both the light-stimulus map and the dark-stimulus map, considered individually, showed a space-time slant appropriate to the direction preference to that stimulus contrast.

Complex direction-selective cells

We recorded from 124 complex direction-selective cells. Some of the complex cells had narrow receptive fields and a response duration around 25 ms or longer (Fig. 6), whereas other complex cells had wider receptive fields and more transient responses (Fig. 7). These probably do not represent two distinct categories, as there was not a bimodal distribution of receptive-field widths (data not shown). The cell in Fig. 2, *C*

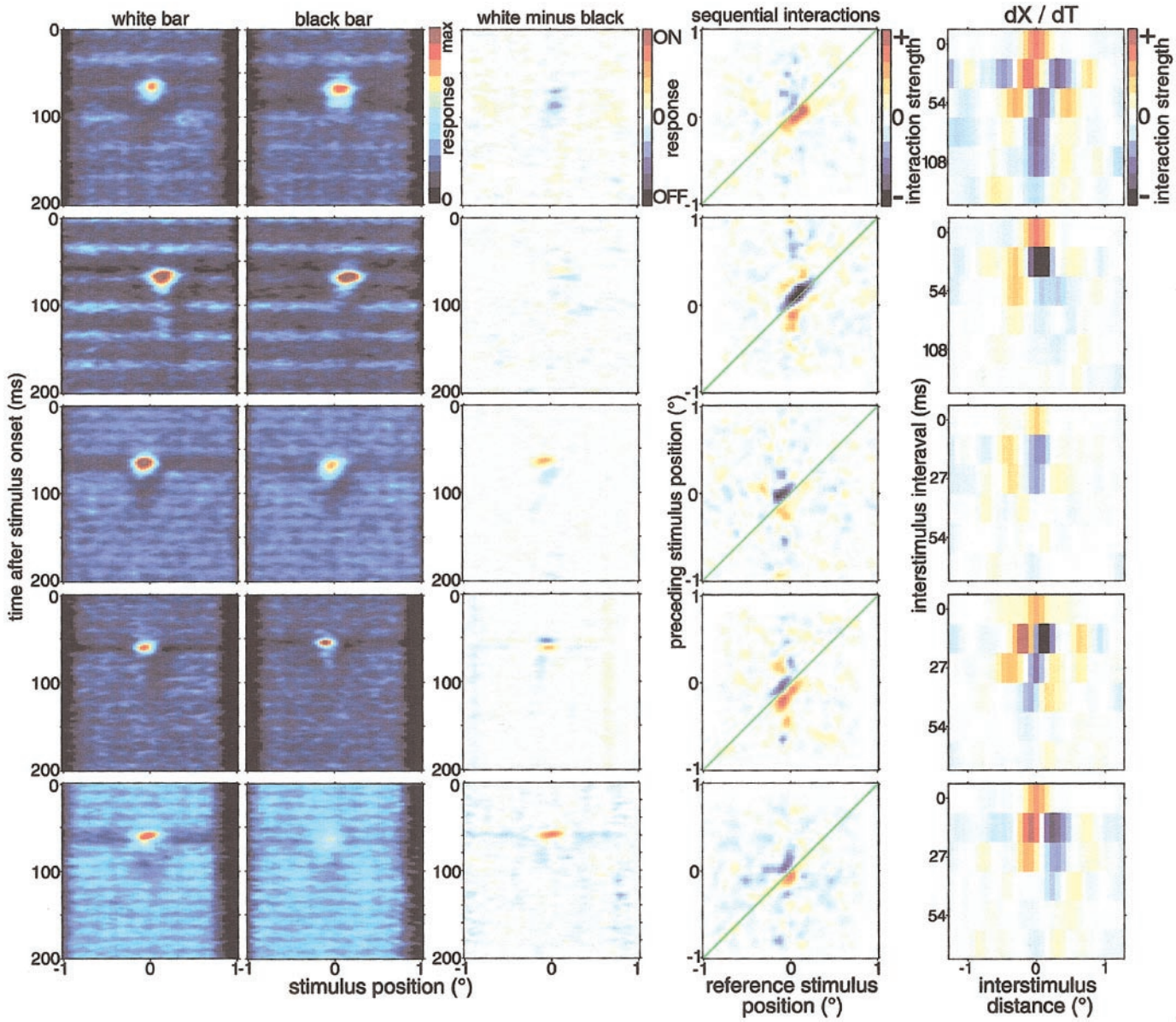

FIG. 6. Space-time maps, sequential interaction maps, and d*X*/d*T* maps for 5 direction-selective complex cells. All these cells had receptive-field eccentricities between 1.5 and 3°. Conventions as in Fig. 4. The white-minus-black maps, included at a reviewer's request, do not distinguish light-excitatory/dark-inhibitory vs. dark-excitatory/light-inhibitory regions as they do for simple cells but rather simply indicate differences in magnitude between ON and OFF influences. For *top 2 cells*, the stimulus presentation rate was 37.5 Hz.

and *D*, and the five cells in Fig. 6 had receptive-field widths about the same size as the width of a single subunit of a conventional simple cell in the population of cells recorded at the same receptive-field eccentricity, 1.5–3°. This group of complex cells had overlapping light and dark excitatory responses, although the light and dark responses were not always of the same magnitude. These cells often showed a region of suppression slightly offset toward the null side of the receptive field (Livingstone 1998). The two-bar interactions showed direction selectivity, which consisted of preferred-direction facilitatory interactions and null-direction suppressive interactions (Figs. 6 and 7, *4th* and *5th columns*).

Some of the complex cells mapped at this eccentricity had relatively wide receptive fields and very transient responses (Fig. 7). Some of these wide complex cells also showed a very shallow slant that was in the same direction as their direction preference, but the slant corresponded to velocities faster than the range to which V1 cells are responsive (Livingstone 1998). The two-bar interactions showed optimum interactions at about the same interstimulus distance as those of the simple cells (Figs. 4 and 5) and the complex cells in Fig. 6, but they were even more elongated (along the +45° diagonal), consistent with their wider receptive fields. Because the range of activation along the vertical or horizontal axes corresponds to the receptive-field width, and the distance from the +45° diagonal corresponds to interstimulus distance, the fact that the directional interactions are narrower perpendicular to the −45° than along the horizontal or vertical axes indicates that the directional interactions must take place in subunits that are narrower than the width of the entire receptive field.

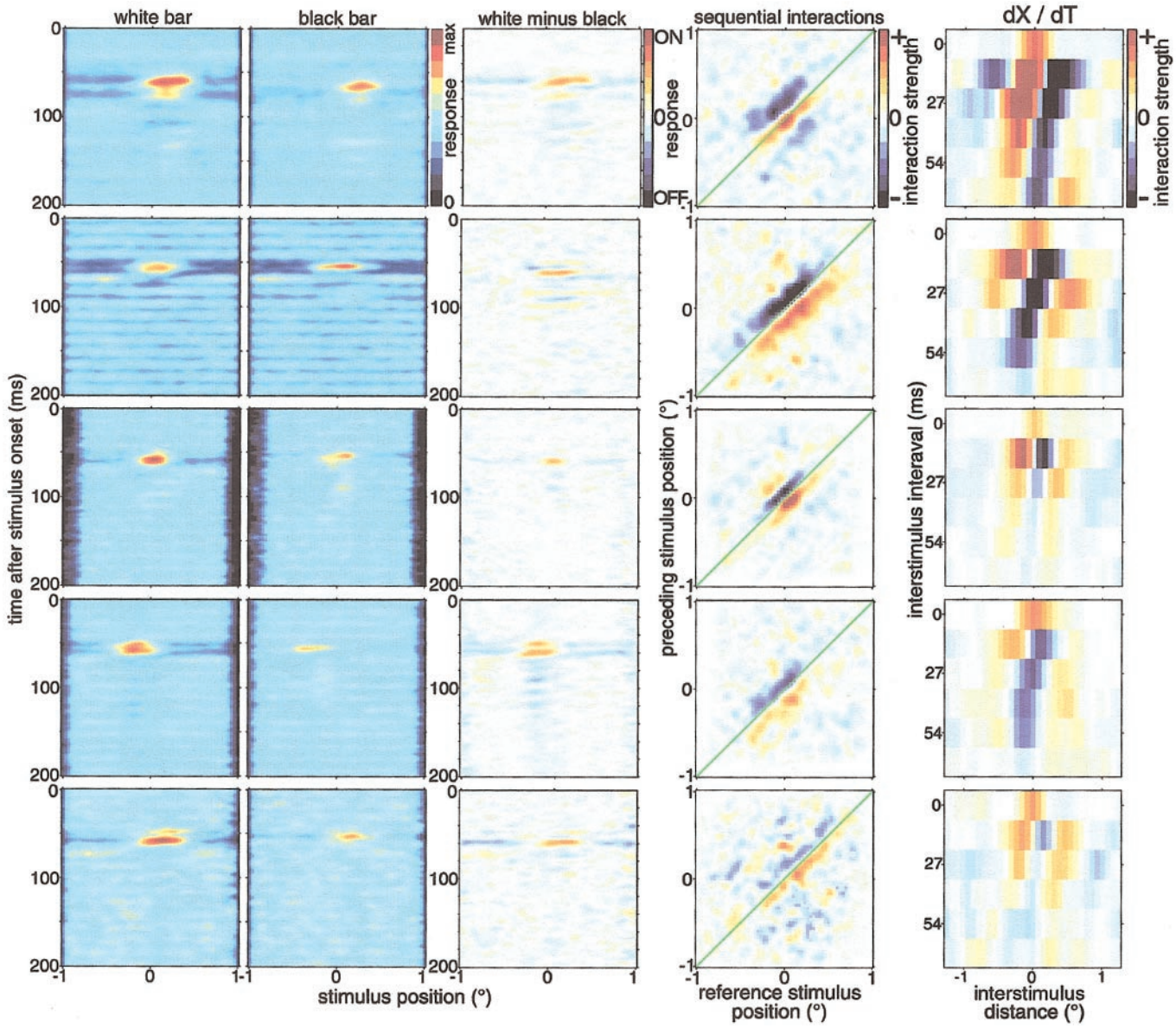

FIG. 7. Space-time maps and sequential interaction maps for 5 direction-selective complex cells with relatively wide receptive fields. All these cells had receptive-field eccentricities between 1.5 and 3°. Conventions as in Fig. 4.

How do our maps fit with various models for direction selectivity?

The idea that the first stage of motion perception is based on space-time slanted filters, such as the simple cells in Fig. 4, was first proposed in two theoretical papers (Adelson and Bergen 1985; Watson and Ahumada 1985). These papers also proposed that such filters could be generated in a linear fashion by summing the responses of nondirectional simple cells (or filters) having spatially and temporally offset receptive fields (Fig. 8, *top*). Although physiological studies have described space-time slanted simple cells, it has been difficult to determine which cell types might represent the nondirectional input cells with different time courses required by the model. The original theoretical papers supposed that the slow component would have the same biphasic time course as the fast component, just delayed by a quarter cycle, as in Fig. 8, *top*.

Two other physiologically reasonable candidates for nondirectional inputs with different time courses have been proposed, one in cats and a different one in primates: De Valois and colleagues (De Valois and Cottaris 1998; De Valois et al. 2000) found in primate V1 two populations of nondirectional simple cells: fast biphasic ones and slower monophasic ones. They determined from principal component analysis that a linear sum of these two classes of nondirectional cells could account for the slant of the space-time maps of the directional cells they mapped. De Valois and Cottaris proposed that magnocellular cells, which are fast and transient, provide the inputs to the fast biphasic inputs in their model, while parvocellular cells, which are slower and more sustained (Dreher et al. 1976; Marrocco 1976; Schiller and Malpeli 1978; Schmolesky et al. 1998), provide the inputs to the slower monophasic component. This model differs from the original energy model in that the slower nondirectional component is temporally monophasic (Fig. 8, *bottom*).

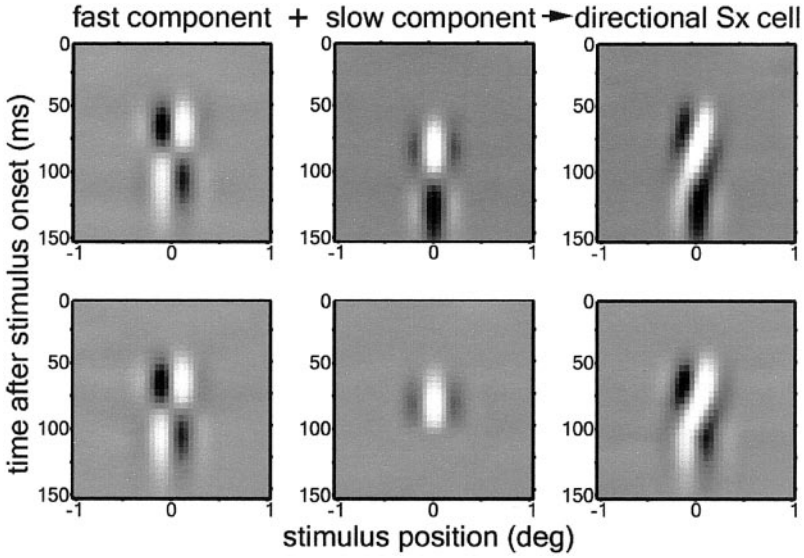

FIG. 8. Models for generating a space-time slanted directional simple cell. Original energy model (*top*) and model with the slow component having a monophasic time course (*bottom*). In both models, the 2 spatial Gabor functions differ in their spatial phase, but they can be modeled as having the same phase and different center positions as in Fig. 10.

In the cat, geniculate cells with appropriately different response time courses have been described—the lagged and nonlagged cells (Mastronarde 1987a,b; Saul and Humphrey 1992; Wolfe and Palmer 1998). Lagged cells are delayed relative to nonlagged cells not because they are slower, as parvo are compared with magno in the monkey, but because, to a sustained stimulus, they reverse response polarity after a short time. However, Wolfe and Palmer (1998) have since suggested that lagged and nonlagged cells are not distinct categories but rather that nonlagged cells are center dominated and lagged cells are surround dominated. Because the initial response in lagged cells is negligible, the response is essentially monophasic, so the lagged-cell model would be similar in principle to the magno/parvo model proposed by De Valois and Cottaris.

Thus physiological findings from anesthetized cat and monkey could be compatible with the original energy model if the model were modified so that the slower component is temporally monophasic and the faster component biphasic. We asked if our recordings in alert monkey also support this idea using principal components analysis.

Principal component analysis of direction-selective simple cells

We analyzed the shape of the simple-cell space-time maps using principal components analysis, as was previously done by De Valois et al. (2000) in anesthetized monkeys. Principal components analysis computes the space-time separable component of the map that accounts for most of its 2-D shape and the amount of additional orthogonal components needed to account for the entire space-time map. DeValois et al. found that their directional simple-cell receptive fields could be decomposed into a temporally biphasic, spatially even-symmetrical, fast component and a slower, temporally monophasic, spatially odd-symmetrical component.

When we did the same analysis on our simple cells recorded in alert monkeys (Figs. 9 and 10), we also found that the receptive fields could be decomposed into a fast, temporally biphasic, component, and a slower, temporally monophasic, component, which together accounted for more than 89% of the shape of each of the maps. However, unlike De Valois et al. (2000), we did not find that the fast component was usually spatially even symmetric and the slow component was usually spatially odd symmetric; indeed, in the five cells analyzed in Fig. 9, which are the same simple cells as in Fig. 4, the fast components are spatially odd-symmetric, and the slower components are even. Figure 10, *top,* shows a summary of the spatial and temporal characteristics of the first two principal components for all the conventional simple cells in our population.(We excluded the single-subunit simple cells from this analysis because their space-time maps did not show much slant, so they did not decompose into two temporally distinct principal components.) *A* and *B* show that in general the faster component was indeed usually temporally biphasic, while the slower component was usually temporally monophasic. *A* also shows that we did not find that the biphasic components were predominantly even symmetric, as reported by De Valois et al. (2000); rather, all spatial phases were represented in both components across the population. *C* shows that the spatial phases of the two components tended to be inversely correlated, but this may be an artifact of using principal components analysis, which requires that the each component be orthogonal to the others. Figure 10, *bottom,* shows that this result could indeed be an artifact of the analysis: two nondirectional model cells, one fast and temporally biphasic (*D*) and the other slower and temporally monophasic (*E*) were summed to generate a model space-time slanted simple cell (*F*). Both the fast and the slow component were spatially odd symmetric (phase angle: 90 °) but were spatially offset by a quarter cycle. Principal components analysis of the "directional" cell (*F*) yielded two components (*G* and *H*) whose time courses corresponded well with the original inputs but whose spatial organization did not correspond to the original inputs. In particular, the slower principal component (*H*) had a 37° phase angle and was thus more even symmetric than odd even though the starting slower monophasic input had a 90° phase angle. This shows that although principal components analysis can accurately decompose temporal components, it may not be able to distinguish between a spatial position shift and a spatial phase shift.

Therefore our result that direction-selective simple cell

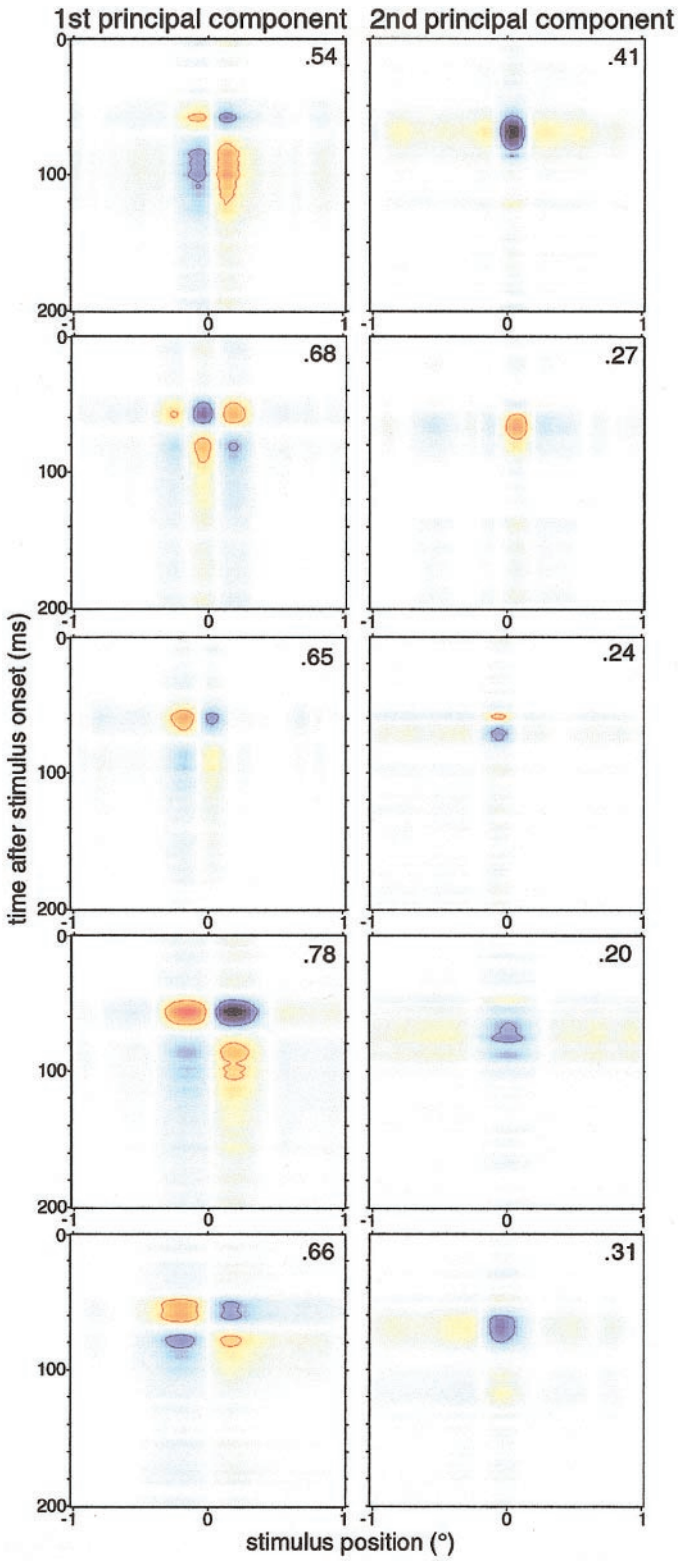

FIG. 9. The 1st 2 principal components for the 5 directional simple cells in Fig. 4. Each row is 1 cell, in the same order as in Fig. 4; same color scheme. The weight of each component (the square of its Eigenvalue) is indicated in the top right corner.

space time maps can be decomposed into a fast temporally biphasic component and a slower monophasic component are in agreement with the results of De Valois et al. (2000), but we believe that the spatial phase of the components is not well determined by PCA.

Relationship between first and second-order maps: space-time slant versus velocity

Space-time slant is a property of the first-order maps, that is, it is a property that depends on only the position and time after each stimulus presentation. Directionality and velocity selectivity are higher-order properties that depend on the spatial and temporal separation of at least two stimuli. The simple cells in Fig. 4 show both space-time slanted first-order maps and slanted second-order dX/dT maps. The direction and slant of the dX/dT maps are similar to the direction and slant of the space-time maps. This similarity may be causal: the slant of the space-time map may be (or may reflect) the mechanism underlying the direction selectivity indicated by the dX/dT map (Adelson and Bergen 1985). To look at the correlation between the first-order space-time (receptive-field) maps and the second-order (direction/velocity) interaction maps, the most obvious question is whether the slants of the space-time maps match the velocity selectivity described by the interaction maps, as they should if the slant produces the direction and velocity selectivity.

This question has previously been asked in anesthetized cat and anesthetized monkey, and in general, the direction and velocity selectivities of cells correlate well with the slants of the space-time maps, although the direction selectivity predicted from the first-order maps usually underestimates the measured magnitude of the direction selectivity. This comparison has been made in several different ways. *1*) Static gratings are presented at different spatial positions to measure first-order responses, which are shifted and summed (superposition) to predict the response to moving gratings (Jagadeesh et al. 1997; Murthy and Humphrey 1999; Reid et al. 1991; Tolhurst and Dean 1991). *2*) Space-time maps are generated using flashed bars, and the slant of the space-time maps is measured using a centriod calculation. This slant is compared with velocity tuning to moving bars (McLean et al. 1994). *3*) Space-time maps are generated using flashed bars, and the predicted velocity tuning is estimated by taking the FFT. This predicted velocity tuning is compared with velocity tuning to moving gratings (Gaska et al. 1994). *4*) Both first- and second-order maps are generated using flashed bars, and they are compared by taking the FFT of each to generate a predicted velocity; both are compared with grating velocity tuning (Baker 2001). *5*) first- and second-order maps are generated using flashed bars, and they are compared by generating a predicted response to moving bars using a half-squaring model; both first- and second-order maps are compared velocity tuning to moving bars (Emerson 1997). Thus there are various ways to measure first-order space-time slant, and various ways to measure second-order spatiotemoral interaction slant, and which one is optimal depends on a number of things, most particularly whether the stimuli were bars or gratings.

Here we compare the *space-time slant* of the first-order maps of all the cells in our population with the *optimum interstimulus distance* in the second-order maps for sequentially presented stimulus pairs (13-ms intervals), with both first- and second-order parameters calculated from the same spike train. For the first-order space-time maps, we measured the slant in several

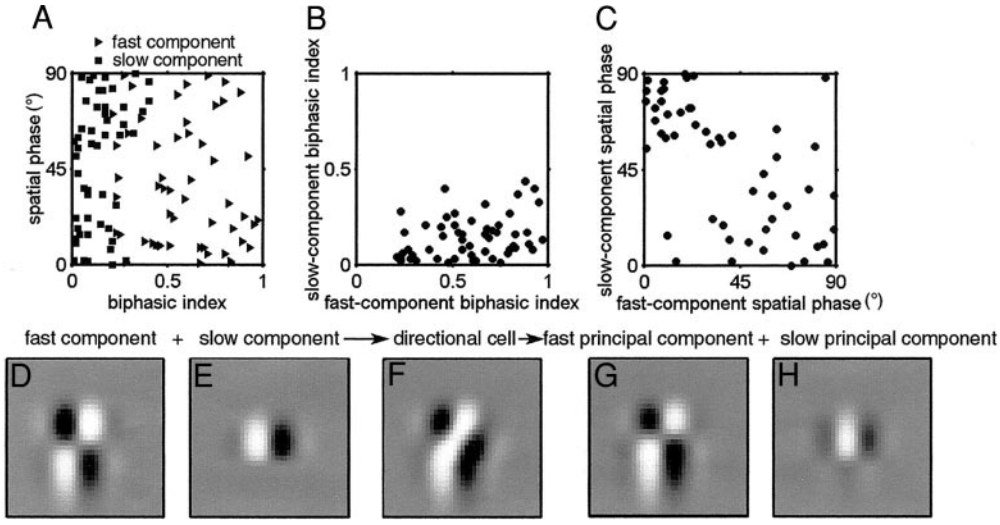

FIG. 10. Relationship between temporal and spatial properties of the 1st 2 principal components of the conventional simple cells. *A*: spatial phase vs. biphasic index for fast and slow principal components. *B*: relationship between biphasic index for the fast and slow principal components for each cell. *C*: relationship between spatial phase for the fast and slow principal components for each cell. *D–H*: principal components analysis of a model simple cell. *D* and *E* show the fast (*D*) and slow (*E*) nondirectional cells that were summed to give a space-time slanted directional simple cell (*F*). The cells in *D* and *E* differ in spatial position rather than in spatial phase, as in Fig. 8. *G* and *H* are the 1st 2 principal components of *F*. *H* does not accurately capture the spatial characteristics of *E*.

different ways, and here we evaluate each of these methods using a simple model. The three ways we compared for measuring first-order space-time slant are the peak of the FFT of the map, which gives you the spatiotemporal frequency with the most power; taking a Radon transform (Deans 1983), which maps the line integral of the image as a function of orientation; and a weighted centroid calculation (a modification of the calculation used by McLean and Palmer 1987) (see METHODS).

For the second-order (interaction) maps, we measured the optimum interstimulus distance for pairs of sequentially presented stimuli divided by 13 ms (the interstimulus interval); this is equivalent to the initial slant (0–13 ms) of the dX/dT plots. The optimum interstimulus separation for sequentially presented stimulus pairs at some interstimulus interval is a definition of velocity tuning to a minimal motion stimulus. Velocity selectivity is usually measured as the optimal dX/dT for a continuously presented moving stimulus. Of course video monitors cannot present a continuous stimulus: a "moving" stimulus on a video monitor consists of flashed stimuli at a series of positions; the optimal velocity is the average interstimulus separation divided by the average interstimulus interval. We measure the optimal interstimulus separation for a 13-ms interval using a minimal motion stimulus—2 flashed bars, which may or may not accurately reflect conventional velocity tuning. A different optimum dX/dT to a series of flashed bars than to a pair of bars would represent an interaction higher than second order.

Figure 11*A* shows a model simple cell we used to explore the correlation between receptive-field space-time slant (1st order) and velocity and direction selectivity (2nd order); this is similar to the model cell in Fig. 8, *bottom*, but with a slightly different spatial phase. *A* shows this model cell's space-time map calculated by subtracting dark responses from light. We have to assume some nonlinearity in this cell's output, otherwise it could not give a direction-selective response to pairs of flashed bars, as our cells do. The nonlinearity we assume for this model is a rectification followed by a squaring (Adelson and Bergen 1985)—a linear filter followed by a static nonlinearity. If we look at this model cell's response to pairs of flashed stimuli presented $t1$ and $t2$ ms (as indicated in Fig. 11*A*) prior to the time of the spikes mapped, we can calculate the nonlinearity due to stimulus pairing (that is the direction and velocity selectivity) by subtracting the inverting-contrast responses from the same contrast (see METHODS). Figure 11*B* shows the pattern of paired-bar interactions for this cell $t2$ ms after the presentation of the second stimulus. This cell shows predominantly positive interactions for preferred-direction sequences (same-contrast facilitation and inverting-contrast suppression) and the reverse for null-direction sequences. Note that these facilitatory and suppressive interactions are arranged in a checkerboard pattern, as observed in some real simple cells (Fig. 4, *top 2 cells*). Collapsing (averaging) a slice parallel to the −45° diagonal of *B* gives us a one-dimensional dX/dT plot of interaction strength as a function of interstimulus distance and interstimulus interval (Fig. 11*C*). This dX/dT map is slanted (that is, the overall Wiener-like kernel is slanted, indicating direction and velocity selectivity). For this model cell, the slant of the light-minus-dark space-time map, measured either by taking its FFT or its Radon transform, corresponds to the average velocity reflected by the dX/dT map. This is to be expected because, in this model, the only mechanism for generating direction selectivity depends on the first-order map.

Figure 11, *A–C*, shows space-time maps and paired-stimulus interactions for light and dark stimuli combined. For the real cells, we measured differences in direction selectivity using light and dark bars independently. Therefore in our model (Fig. 11, *D–I*) we also looked at interactions between pairs of light or pairs of dark stimuli separately. *D* and *G* show the space-time maps for light and dark stimuli independently, assuming the cell rectifies (cannot show negative firing rate). *E* and *H* show the interaction maps for pairs of sequential white stimuli or pairs of sequential black stimuli presented at times $t1$ and $t2$. The interactions for pairs of sequential white stimuli are predominantly facilitatory in the preferred direction and predominantly suppressive in the null direction (Fig. 11*E*). For pairs of black stimuli, however, the interactions are much weaker (Fig. 11*H*). This makes sense, because by inspection the dark-bar space-time map could be matched by both rightward and leftward sequences. The overall dX/dT map for pairs of light bars is predominantly preferred-direction facilitation and null-direction suppression, while the dark bar dX/dT map shows different directionality at different interstimulus distances and intervals. The overall DI (calculated from responses to pairs of

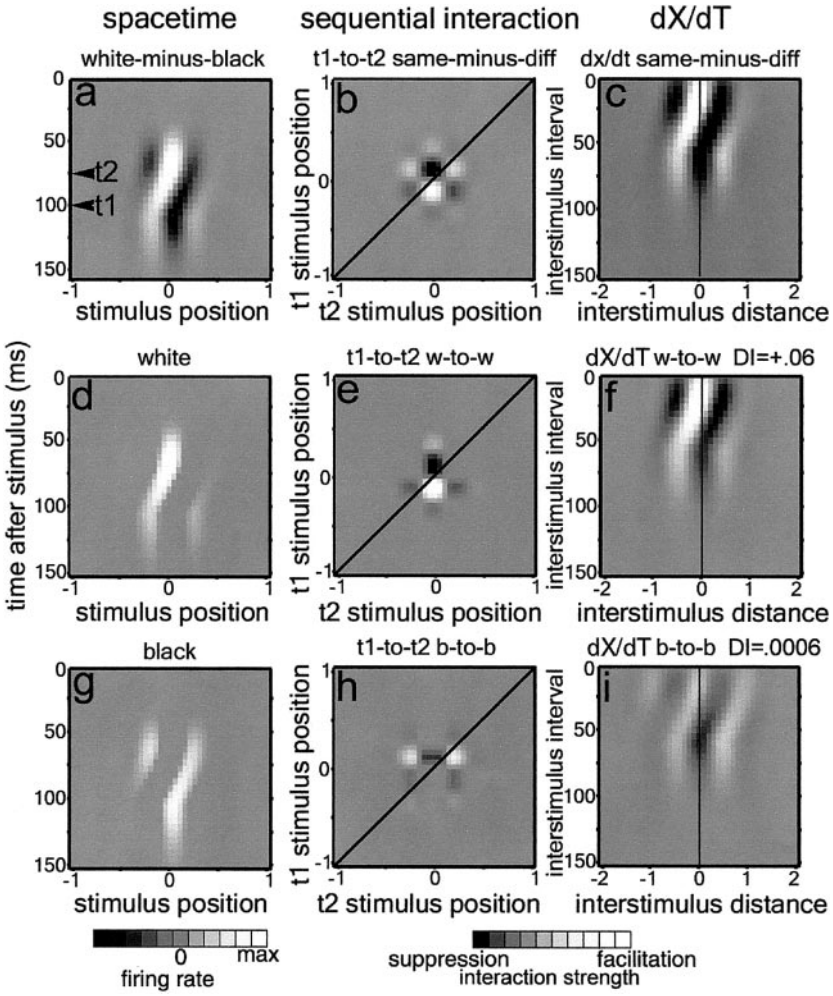

FIG. 11. Exploration of the relationship of space-time slant to direction and velocity selectivity in a model simple cell. *A*: model simple cell; light minus dark responses of a directional simple cell generated by summing 2 nondirectional cells like the 2 in Fig. 8, *bottom*, except slightly phase shifted relative to Fig. 8. *B*: 2-bar interaction map, assuming a rectifying, squaring nonlinearity; same-contrast minus inverting-contrast responses. *C*: d*X*/d*T* map over all possible delays. *D*: rectified white-bar space-time map of this same cell. *E*: 2-bar interaction map for pairs of white bars. *F*: d*X*/d*T* map for pairs of white bars. *G*: rectified black-bar space-time map of this same cell. *H*: 2-bar interaction map for pairs of black bars. *I*: d*X*/d*T* map for pairs of black bars.

bars for all possible interstimulus intervals and distances) for pairs of light bars is rightward (+0.06) but the overall DI for pairs of dark bars is only 0.0006. (The overall direction index is low because responses are calculated for pairs of bars at all possible pairs of positions, not moving bars.) Thus for pairs of dark bars, the directionality is much weaker than for pairs of white bars. This calculation in a simple model is consistent with our finding that many real directional simple cells are directional predominantly to only one stimulus contrast (Fig. 3*D*).

Of the three ways we calculated space-time slant, all three gave appropriate slants for the model simple cell for pairs of light bars; for pairs of dark bars, the FFT slant was in the wrong direction, but the Radon transform and the weighted centriod results were in the correct direction. The preceding results illustrate the difficulty of analyzing space-time slant for two-bar rather than grating stimuli. It is perhaps not surprising that Fourier analysis, being based on sinusoidal components, works for grating stimuli but not for pairs of bars.

In Fig. 12 we compare the slopes of the space-time maps, calculated using a weighted centroid, with the the optimum interstimulus distance per 13-ms interval for those cells that showed significant paired-bar interactions. For conventional simple cells (Fig. 12*A*, ●), the direction of the space-time slant *invariably* correlated with the actual direction selectivity, and the slope of the space-time map correlated roughly with the optimum d*X*/d*T* (slope = 0.43; $r^2 = 0.16$). Fifteen of 18 of the one-subunit simple (S1) cells had a space-time slant that was in the same direction as the actual direction preference, and the slope was slightly less well correlated with the inferred velocity preference (slope = 0.37; $r^2 = 0.16$).

We also looked at complex cells because, as reported previously, complex cells also frequently showed space-time slant that corresponded in direction with the cells' directionality,

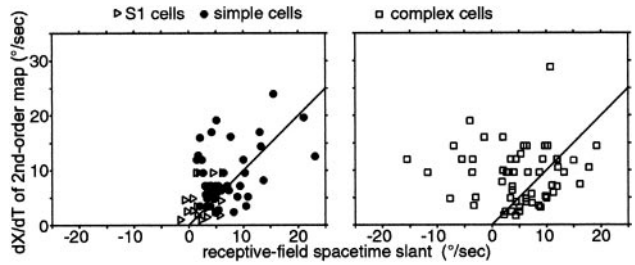

FIG. 12. Correlation between space-time slant and optimum interstimulus distance for a 13-ms interstimulus interval (velocity and direction tuning) for all the cells in our population that showed paired-bar interactions. The space-time slant was calculated from the 1st-order map and the optimum d*X*/d*T* from the 2nd-order map; both calculated from the same spike train. *Left*: conventional simple cells and 1-subunit (S1) simple cells. The single-subunit simple cells generally showed less space-time slant. *Right*: most complex cells also showed a space-time slant that correlated in direction and magnitude with the optimum interstimulus distance for a 13-ms interstimulus interval. The line for $x = y$ is shown for comparison.

though the slant usually corresponded to a much higher velocity than the cell responded to (Livingstone 1998). For the complex cells in this study (*right*) 48 of 59 cells had a space-time slant that was in the same direction as the actual direction preference, but there was no correlation of the slant with the inferred velocity preference (slope = −0.03).

DISCUSSION

Hubel and Wiesel (1962) suggested that cells in cat and primate visual cortex fall naturally into two major categories, simple and complex. In simple cells, light and dark response regions are spatially separate and mutually antagonistic, but in complex cells, they are usually overlapping and not mutually antagonistic. We distinguished simple and complex cells using a metric that we believe captures this original distinction. Our results do not address the issue of whether directional cells in macaque V1 comprise two distinct classes because we did not categorize cells that responded to only one stimulus contrast. Thus we cannot rule out the possibility, suggested by a reviewer, that every cell can be represented by one ON and one OFF Gabor, having the same center, and the relative amplitude of the Gabors varies continuously from positive, through 0, to negative. We point out, however, that Hubel and Wiesel themselves found that not all cells fit neatly into their two categories.

Directional simple cells in macaque V1 had fewer subunits than are commonly seen in the cat, and many of them had only one. Simple cells with only one subunit (S1 cells) were first described by Schiller et al. (1976). However, our population of simple cells showed a continuum in the number and strength of the subunits, so S1 cells represent just one end of this continuum. Ringach (2002) has reported that *nondirectional* simple cells in macaque V1 also show a continuum of subunit number.

We observed directional interactions (nonlinearities) to the simplest possible directional stimulus—two sequentially flashed bars—in both simple and complex cells. The fact that directional interactions in complex cells acted across distances that were shorter than the width of the receptive field implies a subunit structure (Barlow and Levick 1965). This subunit structure is also apparent from the alternating bands of facilitatory and suppressive interactions in complex-cell interaction maps.

The space-time slant of the simple cells correlated with the velocity selectivity inferred from the two-bar sequential interactions. Correlation between direction selectivity and space-time slant has been taken as evidence that the spatiotemporal slant underlies directionality (DeAngelis et al. 1993; McLean and Palmer 1989; McLean et al. 1994; Reid et al. 1991). Complex cell space-time maps were also often slanted, and the direction of the slant often correlated with the preferred direction of motion (though not necessarily with the velocity selectivity). In the energy model, complex cells made up by summing several simple cells would not show any space-time slant if the underlying simple cells were in spatiotemporal quadrature (Emerson et al., 1992). Our finding of some slant in complex cells could reflect the slant of the underlying simple cells if the simple cells were not in perfect quadrature.

De Valois and colleagues (1998, 2000) reported that direction-selective simple cells could be decomposed using principal component analysis into a fast, temporally biphasic, spatially even symmetric component and a slower, temporally monophasic, spatially odd symmetric component. We have confirmed, in alert animals, their observation about the temporal characteristics of the principal components. But we did not observe the spatial distinction they found, and we show that principal components analysis may not be able to distinguish between phase and positional offsets. De Valois and colleagues suggested that the fast component corresponds to simple cells having magnocellular inputs and that the slow component corresponds to cells with parvocellular input because parvocellular responses are more sustained than magnocellular responses. That hypothesis is certainly consistent with both their and our observations, but we would like to suggest that both sets of observations might be better explained by spatially offset inhibition, which also would be expected to have a delayed, temporally monophasic response. That the slow monophasic component is inhibitory, rather than parvocellular in origin, is consistent with observations that GABA blockers abolish direction selectivity in both cat and monkey (Murthy and Humphrey 1999; Sillito 1975, 1977; Tsumoto et al. 1979) and diminish receptive-field space-time slant (Murthy and Humphrey 1999). A delayed offset inhibition model is satisfying because it does not require a separate class of inputs with a slow time course, and it provides a unified mechanism for direction selectivity in both retina and cortex.

D. Freeman developed all the computer programs; T. Chuprina provided excellent technical assistance; C. Pack and D. Tsao provided helpful discussions. C. Pack, D. Tsao, J. Ditterich, and R. Born provided useful software.

This work was supported by National Eye Institute Grant EY-13135 and P30 EY-12196.

REFERENCES

Adelson EH and Bergen JR. Spatiotemporal energy models for the perception of motion. *J Opt Soc Am A Opt Image Sci* 2: 284–299, 1985.

Albrecht DG and Geisler WS. Motion selectivity and the contrast-response function of simple cells in the visual cortex. *Vis Neurosc* 7: 531–546, 1991.

Baker CL Jr. Linear filtering and nonlinear interactions in direction-selective visual cortex neurons: a noise correlation analysis. *Vis Neurosci* 18: 465–485, 2001.

Baker CL and Cynader MS. Space-time separability of direction selectivity in cat striate cortex neurons. *Vision Res.* 28: 239–246, 1988.

Barlow HB and Levick WR. The mechanism of directionally selective units in rabbit's retina. *J Physiol* 178: 477–504, 1965.

Citron MC and Emerson RC. White noise analysis of cortical directional selectivity in cat. *Brain Res* 279: 271–277, 1983.

Conway BR. Spatial structure of cone inputs to color cells in alert macaque primary visual cortex (V-1). *J Neurosci* 21: 2768–2783, 2001.

DeAngelis GC, Ohzawa I, and Freeman RD. Spatiotemporal organization of simple-cell receptive fields in the cat's striate cortex. II. Linearity of temporal and spatial summation. *J Neurophysiol* 69: 1118–1135, 1993.

De Valois RL and Cottaris NP. Inputs to directionally selective simple cells in macaque striate cortex. *Proc Natl Acad Sci USA* 95: 14488–14493, 1998.

De Valois RL, Cottaris NP, Mahon LE, Elfar SD, and Wilson JA. Spatial and temporal receptive fields of geniculate and cortical cells and directional selectivity. *Vision Res* 40: 3685–3702, 2000.

Dean AF and Tolhurst DJ. On the distinctness of simple and complex cells in the visual cortex of the cat. *J Physiol* 344: 305–325, 1983.

Deans SR. *The Radon Transform and Some of its Applications.* New York: Wiley, 1983.

DeAngelis GC, Ohzawa I, and Freeman RD. Spatiotemporal organization of simple-cell receptive fields in the cat's striate cortex. I. General characteristics and postnatal development. *J Neurophysiol* 69: 1091–1117, 1993.

Dreher B, Fukada Y, and Rodieck RW. Identification, classification and anatomical segregation of cells with X-like and Y-like properties in the lateral geniculate nucleus of old-world primates. *J Physiol* 258: 433–452, 1976.

Emerson RC. Quadrature subunits in direcctionally selective simple cells: spatiotemporal interactions. *Vis Neurosci* 14: 357–371, 1997.

Emerson RC, Bergen JR, and Adelson EH. Directionally selective complex cells and the computation of motion energy in cat visual cortex. *Vision Res* 32: 203–218, 1992.

Emerson RC, Citron MC, Vaughn WJ, and Klein SA. Nonlinear directionally selective subunits in complex cells of cat striate cortex. *J Neurophysiol* 58: 33–65, 1987.

Emerson RC and Gerstein GL. Simple striate neurons in the cat. II. Mechanisms underlying directional asymmetry and directional selectivity. *J Neurophysiol* 40: 136–155, 1977.

Ferster D. Spatially opponent excitation and inhibition in simple cells of the cat visual cortex. *J Neurosci* 8: 1172–1180, 1988.

Gaska JP, Jacobson LD, Chen H-W, Pollen DA. Space-time spectra of complex cell filters in the macaque monkey: a comparison of results obtained with pseudowhite noise and grating stimuli. *Vis Neurosci* 11: 805–821, 1994.

Goodwin AW and Henry GH. Direction selectivity of complex cells in a comparison with simple cells. *J Neurophysiol* 38: 1524–1540, 1975.

Hartigan JA and Hartigan PM. The dip test of unimodality. *Ann Stat* 13: 70–84, 1985.

He S and Masland RH. Retinal direction selectivity after targeted laser ablation of starburst amacrine cells. *Nature* 389: 378–382, 1997.

Heeger DJ. Half-squaring in responses of cat striate cells. *Vis Neurosci* 9: 427–443, 1992.

Henry GH. Receptive field classes of cells in the striate cortex of the cat. *Brain Res* 133: 1–28, 1977.

Hirsch JA, Alonso JM, Reid RC, and Martinez LM. Synaptic integration in striate cortical simple cells. *J Neurosci* 18: 9517–9528, 1998.

Hubel DH. Tungsten microelectrode for recording from single units. *Science* 125: 549–550, 1957.

Hubel DH. Single unit activity in striate cortex of unrestrained cats. *J Physiol* 147: 226–238, 1959.

Hubel DH and Wiesel TN. Receptive fields, binocular interaction and functional architecture in the cat's visual cortex. *J Physiol* 160: 106–154, 1962.

Hubel DH and Wiesel TN. Receptive fields and functional architecture of monkey striate cortex. *J Physiol* 195: 215–243, 1968.

Jagadeesh B, Wheat HS, Kontsevitch LL, Tyler CW, and Ferster D. Direction selectivity of synaptic potentials in simple cells of the cat visual cortex. *J Neurophysiol* 78: 2772–2789, 1997.

Livingstone MS. Mechanisms of direction selectivity in macaque V1. *Neuron* 20: 509–526, 1998.

Livingstone MS, Freeman DC, and Hubel DH. Visual responses in V1 of freely viewing monkeys. *Cold Spring Harbor Symp Quant Biol* 61: 27–37, 1996.

Livingstone MS, Pack CC, and Born RT. Two-dimensional substructure of MT receptive fields. *Neuron* 30: 781–793, 2001.

Livingstone MS and Tsao DY. Receptive fields of disparity-selective neurons in macaque striate cortex. *Nat Neurosc* 2: 825–832, 1999.

Marrocco RT. Sustained and transient cells in monkey lateral geniculate nucleus: conduction velocities and response properties. *J Neurophysiol* 39: 340–353, 1976.

Mastronarde DN. Two classes of single-input X-cells in cat lateral geniculate nucleus. I. Receptive-field properties and classification of cells. *J Neurophysiol* 57: 357–380, 1987a.

Mastronarde DN. Two classes of single-input X-cells in cat lateral geniculate nucleus. II. Retinal inputs and the generation of receptive-field properties. *J Neurophysiol* 57: 381–413, 1987b.

Maunsell JH, Ghose GM, Assad JA, McAdams CJ, Boudreau CE, and Noerager BD. Visual response latencies of magnocellular and parvocellular LGN neurons in macaque monkeys. *Vis Neurosci* 16: 1–14, 1999.

Maunsell JH, Nealey TA, and DePriest DD. Magnocellular and parvocellular contributions to responses in the middle temporal visual area (MT) of the macaque monkey. *J Neurosci* 10: 3323–3334, 1990.

McLean J and Palmer LA. Contribution of linear spatiotemporal receptive field structure to velocity selectivity of simple cells in area 17 of cat. *Vision Res* 29: 675–679, 1989.

McLean J, Raab S, and Palmer LA. Contribution of linear mechanisms to the specification of local motion by simple cells in areas 17 and 18 of the cat. *Vis Neurosci* 11: 271–294, 1994.

Mechler F and Ringach DL. On the classification of simple and complex cells. *Vision Res* 42: 1017–1033, 2002.

Movshon JA and Newsome WT. Visual response properties of striate cortical neurons projecting to area MT in macaque monkeys. *J Neurosci* 16: 7733–7741, 1996.

Movshon JA, Thomson ID, and Tolhurst DJ. Spatial summation in the receptive fields of simple cells in the cat's striate cortex. *J Physiol* 283: 53–77, 1978a.

Movshon JA, Thompson ID, and Tolhurst DJ. Receptive field organization of complex cells in the cat's striate cortex. *J Physiol* 283: 79–99, 1978b.

Murthy A and Humphrey AL. Inhibitory contributions to spatiotemporal receptive-field structure and direction selectivity in simple cells of cat area 17. *J Neurophysiol* 81: 1212–1224, 1999.

Murthy A, Humphrey AL, Saul AB, and Feidler JC. Laminar differences in the spatiotemporal structure of simple cell receptive fields in cat area 17. *Vis Neurosci* 15: 239–256, 1998.

Ohzawa I, DeAngelis GC, and Freeman RD. Encoding of binocular disparity by complex cells in the cat's visual cortex. *J Neurophysiol* 77: 2879–2909, 1997.

Reid RC, Soodak RE, and Shapley RM. Directional selectivity and spatiotemporal structure of receptive fields of simple cells in cat striate cortex. *J Neurophysiol* 66: 505–529, 1991.

Ringach D. Spatial structure and symmetry of simple-cell receptive fields in macaque primary visual cortex. *J Neurophysiol* 88: 455–463, 2002.

Saul AB and Humphrey AL. Evidence of input from lagged cells in the lateral geniculate nucleus to simple cells in cortical area 17 of the cat. *J Neurophysiol* 68: 1190–1208, 1992.

Schiller PH, Finlay BL, and Volman SF. Quantitative studies of single-cell properties in monkey striate cortex. I. Spatiotemporal organization of receptive fields. *J Neurophysiol* 39: 1288–1319, 1976.

Schiller PH, Logothetis NK, and Charles ER. Role of the color-opponent and broad-band channels in vision. *Vis Neurosci* 5: 321–346, 1990.

Schiller PH and Malpeli JG. Functional specificity of lateral geniculate nucleus laminae of the rhesus monkey. *J Neurophysiol* 41: 788–797, 1978.

Schmolesky MT, Wang Y, Hanes DP, Thompson KG, Leutgeb S, Schall JD, and Leventhal AG. Signal timing across the macaque visual system. *J Neurophysiol* 79: 3272–3278, 1998.

Sillito AM. The contribution of inhibitory mechanisms to the receptive field properties of neurones in the striate cortex of the cat. *J Physiol* 250: 305–329, 1975.

Sillito AM. Inhibitory processes underlying the directional specificity of simple, complex and hypercomplex cells in the cat's visual cortex. *J Physiol* 271: 699–720, 1977.

Skottun BC, De Valois RL, Grosof DH, Movshon JA, Albrecht DG, and Bonds AB. Classifying simple and complex cells on the basis of response modulation. *Vision Res* 31: 1079–1086, 1991.

Taylor WR, He S, Levick WR, and Vaney DI. Dendritic computation of direction selectivity by retinal ganglion cells. *Science* 289: 2347–2350, 2000.

Tolhurst DJ and Dean AF. Evaluation of a linear model of directional selectivity in simple cells of the cat's striate cortex. *Vis Neurosci* 6: 421–428, 1991.

Tsumoto T, Eckart W, and Creutzfeldt OD. Modification of orientation sensitivity of cat visual cortex neurons by removal of GABA-mediated inhibition. *Exp Brain Res* 34: 351–363, 1979.

Watson AB and Ahumada AJ Jr. Model of human visual-motion sensing. *J Opt Soc Am A Opt Image Sci* 2: 322–341, 1985.

Wiesel TN and Hubel DH. Spatial and chromatic interactions in the lateral geniculate body of the rhesus monkey. *J Neurophysiol* 29: 1115–1156, 1966.

Wolfe J and Palmer LA. Temporal diversity in the lateral geniculate nucleus of cat. *Vis Neurosci* 15: 653–675, 1998.

Yoshida K, Watanabe D, Ishikane H, Tachibana M, Pastan I, and Nakanishi S. A key role of starburst amacrine cells in originating retinal directional selectivity and optokinetic eye movement. *Neuron* 30: 771–780, 2001.

Zar JH. *Biostatistical Analysis.* Upper Saddle River, NJ: Prentice-Hall, 1974.